Synergistic eigenanalysis of covariance and Hessian matrices for enhanced binary classification on health datasets

Agus Hartoyo^{a,c,*}, Jan Argasiński^{a,b}, Aleksandra Trenk^b, Kinga Przybylska^b, Anna Blasiak^{a,b}, Alessandro Crimi^a

^aSano - Centre for Computational Personalized Medicine, Krakow, Poland
 ^bJagiellonian University, Krakow, Poland
 ^cSchool of Computing, Telkom University, Bandung, Indonesia

Abstract

Covariance and Hessian matrices have been analyzed separately in the literature for classification problems. However, integrating these matrices has the potential to enhance their combined power in improving classification performance. We present a novel approach that combines the eigenanalysis of a covariance matrix evaluated on a training set with a Hessian matrix evaluated on a deep learning model to achieve optimal class separability in binary classification tasks. Our approach is substantiated by formal proofs that establish its capability to maximize between-class mean distance and minimize within-class variances, particularly under ideal data conditions such as isotropy around class means and dominant leading eigenvalues. By projecting data into the combined space of the most relevant eigendirections from both matrices, we achieve optimal class separability as per the linear discriminant analysis (LDA) criteria. Empirical validation across neural and health datasets consistently supports our theoretical framework and demonstrates that our method outperforms established methods. Our method stands out by addressing both LDA criteria, unlike PCA and the Hessian method, which predominantly emphasize one criterion each. This comprehensive approach captures intricate patterns and relationships, enhancing classification performance. Furthermore, through the utilization of both LDA criteria, our method outperforms LDA itself by leveraging higher-dimensional feature spaces, in accordance with Cover's theorem, which favors linear separability in higher dimensions. Our method also surpasses kernel-based methods and manifold learning techniques in performance. Additionally, our approach sheds light on complex DNN decision-making, rendering them comprehensible within a 2D space.

Keywords: covariance matrix, Hessian matrix, eigenanalysis, binary classification, class separability

1. Introduction

Binary classification is a fundamental task in machine learning, where the goal is to assign data points to one of two classes. The accuracy and effectiveness of binary classifiers depend on their ability to separate the two classes accurately. However, achieving optimal class separability can be challenging, especially when dealing with complex and high-dimensional data.

Traditional approaches often rely on analyzing either the covariance matrix [1, 2, 3, 4, 5, 6, 7] or

the Hessian matrix [8, 9, 10, 11, 12, 13, 14] separately to optimize machine learning models. In the field of Evolution Strategies (ESs), a recent work [15] explored the relationship between the covariance matrix and the landscape Hessian, highlighting the statistical learning capabilities of ESs using isotropic Gaussian mutations and rank-based selection. While this study provides valuable insights into ESs' learning behavior, it does not investigate the practical integration of the two matrices.

When analyzing the covariance matrix, the focus is on capturing the inherent patterns of variability within the data, allowing for a compact representation that highlights relationships between different dimensions. On the other hand, the analysis of the

^{*}Corresponding author. Sano - Centre for Computational Personalized Medicine, Czarnowiejska 36 building C5, 30-054 Kraków. E-mail address: a.hartoyo@sanoscience.org

Hessian matrix aims to find the direction in which the classes are best separated, by maximizing the curvature along the discriminative directions. However, these separate analyses fail to fully leverage the synergistic effects that can arise from integrating the information contained in both matrices.

To tackle this challenge, we present a novel approach that combines the eigenanalysis of the covariance matrix evaluated on a training set with the Hessian matrix evaluated on a deep learning model. By integrating these matrices, our method aims to optimize class separability by simultaneously maximizing between-class mean distance and minimizing within-class variances, which are the fundamental criteria of linear discriminant analysis (LDA) [16, 17]. By utilizing these criteria, we leverage the foundational principles that have been established and proven over decades of LDA's application in various fields like medicine [18, 19, 20, 21, 22], agriculture [23, 24, 25, 26, 27], and biometrics [28, 29, 30, 31, 32, 33, 34]. LDA has been demonstrating the reliability and usefulness of the two criteria as indicators of discriminative power. Thus, by building upon this well-established foundation, our approach will inherit the strengths and reliability that have been demonstrated by LDA. This integrated approach holds the promise of enhancing classification performance beyond conventional methods that treat the two matrices separately.

Clustering algorithms [35, 36, 37, 38, 39, 40, 41, 42, 43, 44, 45, 46] also adhere to principles similar to those of LDA criteria. Just as our proposed method leverages the LDA criteria for optimizing class separability by maximizing between-class mean distance and minimizing within-class variances, clustering techniques aim to enhance cluster separability by maximizing both inter-cluster dissimilarity (the concept of separation) and intra-cluster similarity (the concept of compactness) [47, 48, 49, 50]. This alignment highlights the effectiveness and utility of LDA criteria in various data analysis techniques, demonstrating that these principles are broadly applicable and beneficial for achieving distinct and compact data groupings.

2. Methodology

2.1. Approach: combining eigenanalysis of covariance and Hessian matrices

In this subsection, we describe our novel approach for combining the eigenanalysis of the covariance matrix and the Hessian matrix to achieve

optimal class separability in binary classification tasks.

1. Covariance matrix eigenanalysis: A covariance matrix $Cov(\theta)$ is a $D \times D$ matrix, where D represents the dimensionality of the predictor attributes. Each element of the covariance matrix reflects the covariance between the two predictor attributes θ_1 and θ_2 :

$$Cov(\theta_1, \theta_2) = \frac{1}{n-1} \sum_{i=1}^{n} (\theta_{1i} - \bar{\theta}_1)(\theta_{2i} - \bar{\theta}_2)$$
 (1)

where θ_{1i} and θ_{2i} are the corresponding observations of these predictor attributes for the *i*-th data instance, $\bar{\theta}_1$ and $\bar{\theta}_2$ are the sample means of the predictor attributes θ_1 and θ_2 , respectively, and n is the number of data instances or observations.

Performing eigenanalysis on the covariance matrix $Cov(\theta)$, we obtain eigenvalues λ_i and corresponding eigenvectors \mathbf{v}_i . The leading eigenvector \mathbf{v}_1 associated with the largest eigenvalue λ_1 , as captured in the eigenequation $Cov(\theta) \cdot \mathbf{v}_1 = \lambda_1 \cdot \mathbf{v}_1$, represents the principal direction with the highest variance.

2. Hessian matrix eigenanalysis: Next, we compute a Hessian matrix evaluated on a deep learning model trained on the same training set. We employ a deep neural network (DNN) architecture consisting of four fully connected layers, each followed by a Rectified Linear Unit (ReLU) activation. The final layer employs a sigmoid activation function to yield a probability value within the range of 0 to 1. During training, we utilize the binary cross-entropy loss function. The binary cross-entropy loss is given by

BCELoss =
$$-\sum_{i=1}^{n} \log p_{\theta}(c_i \mid x_i),$$
 (2)

where c_i is the actual class for data instance x_i . The probability $p_{\theta}(c_i \mid x_i)$ is the predicted probability of instance x_i belonging to class c_i , as estimated by the DNN model parameterized by θ .

The Hessian of the loss function is then:

$$H_{\theta} = \nabla_{\theta}^{2} \text{BCELoss}$$

$$= \nabla_{\theta}^{2} \left[-\sum_{i=1}^{n} \log p_{\theta}(c_{i} \mid x_{i}) \right]$$

$$= -\sum_{i=1}^{n} \left[\nabla_{\theta}^{2} \log p_{\theta}(c_{i} \mid x_{i}) \right].$$
(3)

Performing eigenanalysis on the Hessian matrix H_{θ} , we obtain eigenvalues λ'_i and corresponding eigenvectors \mathbf{v}'_i . The leading eigenvector \mathbf{v}'_1 associated with the largest eigenvalue λ'_1 , as captured in the eigen-equation $H_{\theta} \cdot \mathbf{v}'_1 = \lambda'_1 \cdot \mathbf{v}'_1$, represents the direction corresponding to the sharpest curvature.

3. Integration of matrices and projection of data: To combine the power of covariance and Hessian matrices, we project the data into the combined space of the most relevant eigendirections. Let U be the matrix containing the leading eigenvectors from both matrices:

$$\mathbf{U} = [\mathbf{v}_1, \mathbf{v}_1'] \tag{4}$$

The 2D projection of the data, denoted as $\mathbf{X}_{\mathrm{proj}}$, is obtained by:

$$\mathbf{X}_{\text{proj}} = \mathbf{X} \cdot \mathbf{U} \tag{5}$$

Here, X is the original data matrix, and $X_{\rm proj}$ represents the final output of the proposed method—a 2D projection capturing both statistical spread and discriminative regions of the data.

Unlike LDA, which aims to optimize both criteria simultaneously along a single direction for binary classification, constrained by the limitation that the number of linear discriminants is at most c-1 where c is the number of class labels [51], our approach provides more flexibility and control. By working on two separate directions, we specifically focus on minimizing the within-class variances in one direction while maximizing the between-class mean distance in the other direction.

2.2. Formal foundation: maximizing the squared between-class mean distance and minimizing the within-class variance

In this subsection, we establish two theorems along with their respective proof sketches that form the theoretical basis for our approach. Full proofs for both theorems are available in Appendix A.

2.2.1. Theorem 1: Maximizing covariance for maximizing squared between-class mean distance.

Consider two sets of 1D data points representing two classes, denoted as C_1 and C_2 , each consisting of n samples. The data in C_1 and C_2 follow the same underlying distribution centered around their respective means, m_1 and m_2 . Here, C_2 can be understood as a reflection of C_1 with the axis of reflection positioned at the overall mean, denoted as m. Furthermore, the variances of C_1 and C_2 are equal, denoted as $\sigma_1^2 = \sigma_2^2 = \sigma_w^2$, and the combined data from C_1 and C_2 has a variance of σ^2 . The between-class mean distance, denoted as d, represents the separation between the means of C_1 and C_2 . We establish the following relationship:

$$\sigma^2 = \frac{d^2}{4(1-\lambda)}\tag{6}$$

where $\lambda = \frac{\sigma_w^2}{\sigma^2}$ signifies a constant between 0 and 1 that reflects the distribution of the original data when C_1 and C_2 are considered as projected representations.

Proof sketch:.

- 1. Consider two classes C_1 and C_2 with identical underlying distributions.
- 2. Simplify the expression for the combined data variance σ^2 to $\sigma_w^2 + \frac{1}{4}d^2$.
- 3. Apply the Variance Ratio Preservation Theorem for Projection onto a Vector to relate σ_w^2 and σ^2 through λ .
- 4. Simplify the expression to obtain $\sigma^2 = \frac{d^2}{4(1-\lambda)}$.
- 5. Conclude that maximizing σ^2 maximizes d^2 , fulfilling the theorem's objective.

In the context of multidimensional data, extending Theorem 1 involves considering data points as D-dimensional vectors, where the dataset consists of two subsets, $C_1 = \{\vec{x}_i \in \mathbf{R}^D \mid i = 1, 2, \dots, n\}$ with covariance Cov_1 , and $C_2 = \{\vec{y}_j \in \mathbf{R}^D \mid j =$ $1, 2, \ldots, n$ } with covariance Cov_2 . The theorem, however, is supposed to hold for the projection of the data onto an arbitrary 1D subspace of the full D-dimensional data space, and to imply that maximizing σ^2 by choosing the direction of this subspace appropriately will also be the direction that maximizes the difference between the projected sample means. A general case in which it holds is when the individual distributions are isotropic about their means, meaning the covariances Cov_1 and Cov_2 are proportional to the identity matrix in D dimensions as mathematically shown in Appendix B.

2.2.2. Theorem 2: Maximizing Hessian for minimizing within-class variance

Let θ be a parameter of the model, and H_{θ} denote the Hessian of the binary cross-entropy loss function with respect to θ . We define the withinclass variance as the variance of a posterior distribution $p_{\theta}(\theta \mid c_i)$, which represents the distribution of the parameter θ given a class c_i . We denote the variance of this posterior distribution as σ_{post}^2 . We establish the following relationship:

$$H_{\theta} = \frac{1}{\sigma_{\text{post}}^2}.$$
 (7)

Proof sketch:.

- 1. Consider the parameter θ and the Hessian H_{θ} of the binary cross-entropy loss function. Define the within-class variance σ_{post}^2 as the variance of the posterior distribution $p_{\theta}(\theta \mid c_i)$.
- 2. Approximate the Hessian H_{θ} as the Fisher information using the expectation of the squared gradient of the log-likelihood [52].
- 3. Assume a known normal likelihood distribution for $p_{\theta}(c_i \mid \theta)$ with mean μ and standard deviation σ . Compute the Fisher information as $\frac{1}{\sigma^2}$.
- 4. Considering a uniform prior distribution $p(\theta)$ within the plausible range of θ and the evidence $p(c_i)$ as a known constant, apply Bayes' formula to derive that $\sigma_{\text{post}}^2 = \sigma^2$.
- 5. Derive $H_{\theta} = \frac{1}{\sigma_{\text{post}}^2}$.
- 6. Conclude that maximizing H_{θ} minimizes σ_{post}^2 , achieving the theorem's objective.

Theorem 1 and Theorem 2 respectively suggest that maximizing the variance of projected data and the Hessian effectively maximize squared betweenclass mean distance and minimize within-class variances, contingent upon the ideal data conditions discussed in Section 3. These theorems provide the theoretical foundation for the eigenanalysis of the covariance and Hessian matrices, crucial steps in our proposed method for improving class separability based on the two LDA criteria.

3. Ideal dataset conditions for the optimal performance of the proposed method

To ensure the optimal performance of the proposed method, it is crucial to consider certain ideal

conditions for the dataset. These conditions represent ideal scenarios that can help achieve optimal performance and support the theoretical foundations of the method. The key conditions are as follows:

- 1. Isotropic distributions around class means:
 - The theoretical underpinnings of the proposed method, particularly in the application of Theorem 1 to multidimensional data, benefit from the dataset subsets corresponding to each class being approximately isotropic around their respective means, as mathematically shown in Appendix B. While perfect isotropy—where the covariance matrices of the subsets are proportional to the identity matrix in D dimensions—is rare in practice, achieving nearisotropic conditions helps ensure the validity of the theorem to higher dimensions and the method's ability to leverage the relationship between covariance and class separability.

In more practical terms, datasets tend to support isotropism under the following conditions:

- (a) Normalized data: Normalizing the data, typically through techniques such as zscore normalization, ensures that each attribute has a mean of zero and a standard deviation of one. This process equalizes variance in all directions, which approximates the isotropic condition.
- (b) Low correlation between attributes:

 Datasets with low correlation between attributes produce covariance matrices with minimized off-diagonal elements.

 This condition approximates isotropy, which is characterized by covariance matrices being proportional to the identity matrix.
- 2. Dominance of the first eigenvalues in covariance and Hessian matrices:

The effectiveness of the proposed method is heavily reliant on the information provided by the leading eigenvectors derived from the covariance and Hessian matrices. For these matrices to significantly contribute to the method's success, their first eigenvalues need to be sufficiently dominant. A dominant first eigenvalue indicates that the corresponding eigenvector captures the most significant variance or curvature in the data, making it a crucial direction for class separation.

The presence of a dominat first eigenvalue can be assessed from the eigenspectra of the two matrices, which display the eigenvalues on a log scale. A dominant first eigenvalue is characterized by the eigenvalues being spread over many orders of magnitude, often with approximately uniform spacing between them. When a dominant first eigenvalue is present in the covariance matrix, it suggests a dominant underlying structure or trend in the data. When this occurs in the Hessian matrix, it characterizes a "sloppy" model [53, 54, 55, 56, 57, 58, 59], which has a few stiff directions (significant eigenvalues) and many sloppy directions (small eigenvalues).

4. Complexity analysis

In assessing the computational demands of our proposed method, we employ big O notation to describe the worst-case time complexity. The overall time complexity of our method encompasses several tasks, including covariance and Hessian matrix computations $(\mathcal{O}(N \cdot F^2))$, eigenanalysis of these matrices $(\mathcal{O}(F^3))$, selection of eigenvectors corresponding to leading eigenvalues $(\mathcal{O}(1))$, and data projection into the combined space $(\mathcal{O}(N \cdot F))$. Here, N signifies the number of data points in the training set, while F represents the number of features per data point. It is essential to note that this analysis considers our method's computational demands under the assumption that a pre-existing DNN is in place.

Comparatively, the time complexity of LDA is primarily influenced by the calculation of both within-class and between-class scatter matrices $(\mathcal{O}(N\cdot F^2))$ and subsequent eigenanalysis $(\mathcal{O}(F^3))$. In both methods, the dominant complexity factor is either the matrix computations $(\mathcal{O}(N\cdot F^2))$ when there are more examples than features or the eigenanalysis step $(\mathcal{O}(F^3))$ otherwise.

This analysis reveals that our proposed method exhibits a comparable computational profile to the method under improvement. Therefore, our approach offers enhanced class separability and interpretability without significantly increasing computational demands, making it a practical choice for real-world applications.

5. Experiment

5.1. Assessed dimensionality reduction techniques

In our evaluation, we compare nine distinct dimensionality reduction and data projection techniques, each offering unique insights: principal component analysis (PCA), kernel PCA (KPCA) [60], Hessian, uniform manifold approximation and projection (UMAP) [61], locally linear embedding (LLE) [62], linear optimal low-rank projection (LOL) [63], linear discriminant analysis (LDA), kernel discriminant analysis (KDA) [64], and the proposed approach. PCA involves projection onto the primary two covariance eigenvectors, i.e., it applies KPCA with a linear kernel. Similarly, LDA employs KDA with a linear kernel. The Hessian method projects data onto the leading two Hessian eigenvectors. Notably, for both KPCA and KDA, the best kernels (linear, polynomial, RBF, sigmoid, or cosine similarity) and their associated parameters (kernel coefficient or degree) are determined using grid search tailored to each dataset. The proposed method combines the most relevant eigenvectors derived from both the covariance and Hessian matrices, as specified by Eqs(4, 5).

5.2. Class separability assessment via linear SVMs

The nine dimensionality reduction methods we assess are designed to transform high-dimensional data into more manageable 1D or 2D spaces while simultaneously enhancing or preserving class separability. Linear SVMs enable us to create decision boundaries that are readily visualized in these 1D or 2D spaces. Thus, we utilize SVMs with a linear kernel to evaluate and visualize the extent of class separability achieved through the projections.

In addition to the visualization of decision boundaries, we employ a comprehensive set of evaluation metrics to quantify the performance of the dimensionality reduction methods. These metrics include the F1 score, which measures the balance between precision and recall, the Area Under the Receiver Operating Characteristic Curve (AUC ROC), which assesses the model's ability to distinguish between positive and negative classes, and Cohen's kappa, a statistic that gauges the agreement between the predicted and actual class labels.

5.3. Datasets

We will conduct our assessment of the nine distinct methods on the following datasets:

Widely recognized benchmark datasets. We evaluate our approach using three widely recognized benchmark datasets for binary classification: the Wisconsin breast cancer dataset [65], the heart disease dataset [66], and the Pima Indians diabetes

dataset [67]. Prior to applying various dimensionality reduction methods, we enact standard data preprocessing techniques on the original datasets, including handling of missing data, one-hot encoding for categorical variables, and data normalization. Specifically, we apply z-score normalization to ensure the data has zero mean and unit variance, supporting the requirement for the data to be isotropic as suggested in Section 3.

Neural spike train dataset. A spike train is a sequence of action potentials (spikes) emitted by a neuron over time. The neural spike train dataset used in this research consists of recordings from rat's neurons during drug application from a multi-electrode array [68, 69]. The data, comprising 221 records, represents the final dataset after all pre-processing steps suggested by [70]. Each record contains 15 time-series features extracted using the 'tsfresh' package [71] and 1 class attribute indicating whether the neuron is non-responsive (0) or responsive (1). Exploratory data analysis revealed an imbalance in the dataset, with 190 non-responsive neurons (86%) and 31 responsive neurons (14%).

To provide an unbiased assessment of our method's performance, we conduct extensive experiments on the datasets with 10-fold cross-validation with the exception of the neural spike train dataset. Due to the limited number of positive cases in the neural spike train dataset, we performed 5-fold cross-validation to ensure a reasonable sample size for validation.

5.4. Results

The results depicted in Figure 1, which pertain to the WBCD dataset, along with the corresponding findings presented in Appendix C for the other three datasets, collectively reaffirm the consistency and robustness of our proposed approach across diverse datasets. The heatmaps shown in Figure 1(b) and Appendix C consistently demonstrate the reduction in squared between-class mean distance as more covariance eigenvectors are incorporated. aligning with our established theoretical framework (Eq(6)). Furthermore, Figure 1(c) and its counterparts in the appendix reveal the ascending order of within-class variances, in sync with the descending order of the Hessian, supporting our theoretical foundation (Eq(7)). Furthermore, Figure 1(d) and its counterparts illustrate the LDA ratio, emphasizing the equal contributions of covariance and Hessian eigenanalyses to class separability. Importantly, the results also imply that the highest LDA ratio is observed for the combination of the first Hessian eigenvector with the first covariance eigenvector. This observation underscores the significance of projecting data onto the combined space of these primary eigenvectors (as outlined in Eqs (4, 5)), forming the core of our proposed method. These consistent empirical results across multiple datasets not only validate our theoretical premises but also endorse the effectiveness of our proposed method in optimizing class separability.

The evaluation results in Figure 2 compare the performance of different data projection methods. including PCA, KPCA, Hessian, UMAP, LLE, LOL, LDA, KDA, and the proposed method, using 5- or 10-fold cross-validation. It is essential to note that we introduced nonlinearity to the comparative analysis by utilizing distinct kernels determined through grid search in KPCA and KDA for each dataset. Notably, our proposed method consistently outperforms all others, securing the highest average scores across all datasets and evaluation metrics. This consistent superiority of our approach implies its potential as a valuable tool for improving classification performance in various domains, further highlighting its promise as a robust and effective method for dimensionality reduction and data projection.

6. Illustrative case study: WBCD dataset

In this section, we illustrate the practical application of the proposed method using the WBCD dataset. The WBCD dataset comprises 30 predictor attributes for diagnosing breast cancer. This section presents detailed analyses and visualization of the WBCD dataset using our method and other established data projection techniques.

We first examine the separability of classes in the WBCD dataset using basic pairwise attribute projections. Figure 3 shows a pairplot of the first four predictor attributes, colored by class labels. This pairplot projects the 30-dimensional data into 1D and 2D spaces between individual attributes and attribute pairs. As can be visually observed from the figure, these simple projections do not provide good separability between the two classes. This is because these projections are not optimized for class separability. In contrast, established projection methods such as PCA, LDA, and UMAP, as well as our proposed method, are specifically designed and optimized to enhance class separability.

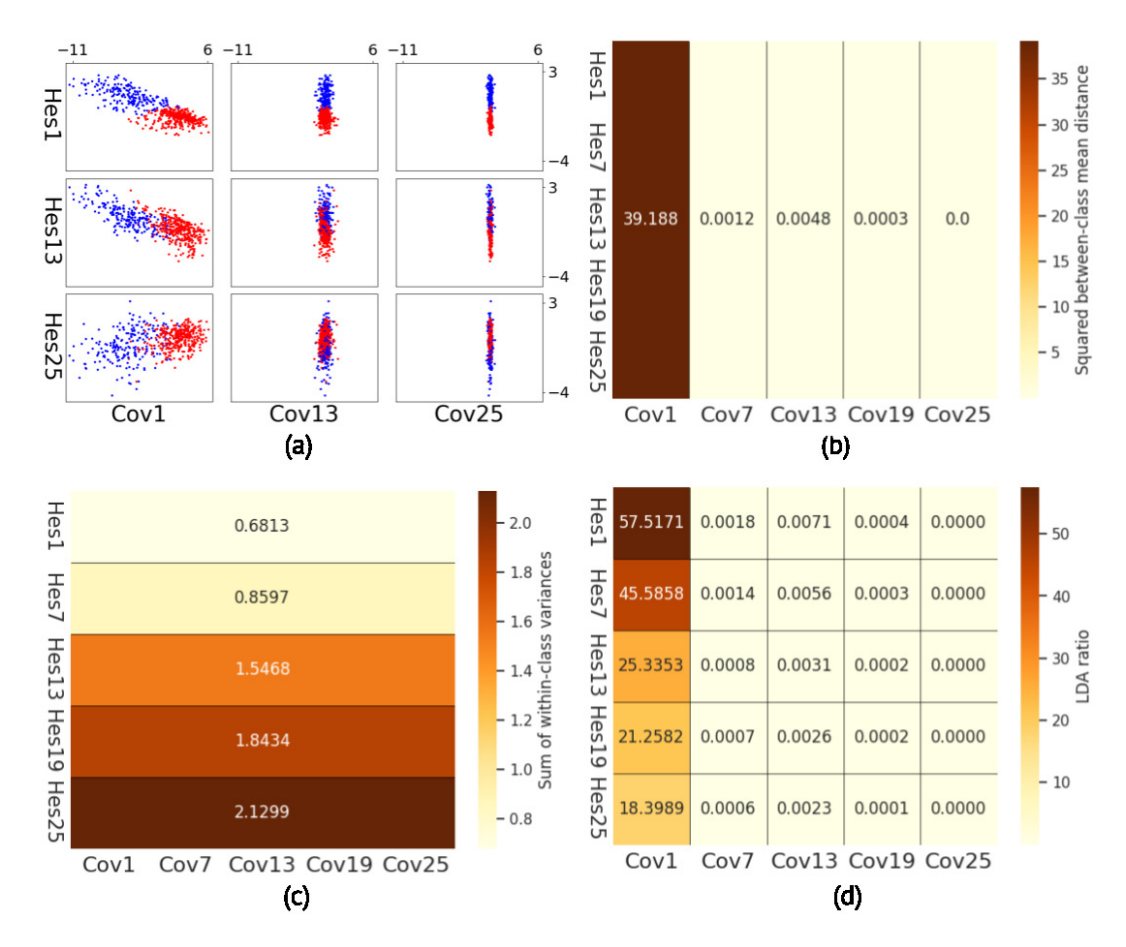


Figure 1: Projection of the Wisconsin breast cancer data into different combined spaces of the covariance and Hessian eigenvectors. (a) Nine selected projection plots, each representing data projected onto a distinct space created by combining the first three covariance and first three Hessian eigenvectors. (b) Heatmap showing the squared between-class mean distance for projections onto varying combinations of covariance and Hessian eigenvectors. The heatmap demonstrates that the values remain constant vertically across different Hessian eigenvectors, while exhibiting a noticeable descending order horizontally, aligning with the descending order of the variance. These results essentially concretize our formal premise, empirically validating the linear relationship described in Eq(6) between the variance and the squared between-class mean distance. (c) Heatmap showing the sum of within-class variances for projections onto different combinations of covariance and Hessian eigenvectors. The values remain constant horizontally across different covariance eigenvectors but exhibit a clear ascending order vertically, aligning with the descending order of the Hessian. These empirical results validate the negative correlation between the Hessian and the within-class variance described in Eq(7) within the framework of our theoretical foundation. (d) Heatmap displaying the LDA ratio, representing the ratio between the squared between-class mean distances presented in (b) and the corresponding within-class variances shown in (c). The highest LDA ratio is observed for the combination of the first Hessian eigenvector with the first covariance eigenvector. Notably, a general descending pattern is observed both horizontally and vertically across different combinations, indicating that both covariance eigenanalysis (represented along the horizontal direction) and Hessian eigenanalysis (represented along the vertical direction) equally contribute to the class separability (represented by the LDA ratio).

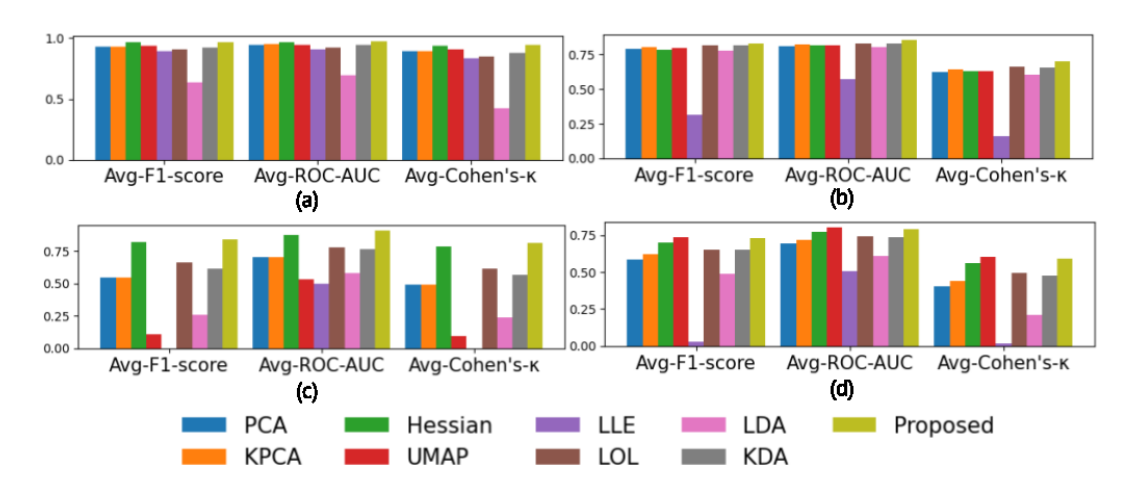


Figure 2: Performance comparison of data projection methods using cross-validation on four distinct datasets: (a) WBCD, (b) heart disease, (c) neural spike train, and (d) Pima Indians diabetes datasets. This figure presents the average F1 score, ROC AUC, and Cohen's Kappa values obtained through 5- or 10-fold cross-validation for nine data projection techniques: PCA, KPCA (cosine similarity for WBCD, polynomial kernel with degree=3 for Heart, linear kernel for Neural, cosine similarity for Pima), Hessian, UMAP, LLE, LOL, LDA, KDA (cosine similarity for WBCD, RBF kernel with coefficient=0.01 for Heart, sigmoid kernel with coefficient=2 for Neural, cosine similarity for Pima), and the proposed method. Notably, the proposed method consistently outperforms all other techniques, achieving the highest scores across all evaluation metrics.

Our proposed method leverages the strengths of both the covariance matrix and the Hessian matrix to achieve optimal class separability. Figure 4 presents the heatmaps of the covariance and Hessian matrices computed from the WBCD dataset. The covariance matrix, computed unsupervisedly from the training set using Eq. 1, is a square and symmetric matrix that captures the statistical spread and relationships between predictor attributes. The Hessian matrix, evaluated on a deep learning model trained on the same training set using Eq. 3, is another square and symmetric matrix that reflects the sensitivity and curvature of the loss function with respect to the model parameters. The DNN test scores are as follows: accuracy: 0.9883, F1 score: 0.9841, AUC ROC: 0.9917, Cohen Kappa score: 0.9749, geometric mean score: 0.9874.

By performing eigenanalysis on the covariance and Hessian matrices, we obtain leading eigenvectors that represent the principal directions of variance and the sharpest curvature, respectively. These eigendirections are crucial for projecting the high-dimensional data into a 2D space that enhances class separability by maximizing the between-class mean distance and minimizing the within-class variances, as described in Theorem 1 and Theorem 2. We project the data into the combined space of the two eigendirections using Eq. 4 and Eq. 5. Figure 5 visually demonstrates the ef-

fectiveness of the proposed method by showing the 2D projections of the WBCD dataset. The training set projection highlights the observed visual separation achieved on the training data, while the test set projection confirms good visual separability for new unseen data, underscoring the method's potential to generalize well. The visual separability observed here will be quantified later using SVM (Figures 7 and 8).

Our proposed method not only enhances class separability but also facilitates interpretability and explainability of the model. Figure 6 presents the parameter contributions to the leading eigenvectors of the covariance and Hessian matrices for the WBCD dataset. The contributions are calculated as the absolute values of the elements in the first eigenvector of each matrix. Parameters are sorted by their absolute contributions, and the horizontal bar plots display these sorted contributions for each parameter. The first plot indicates which attributes contribute the most to maximizing the betweenclass mean distance, providing insights into the key factors that drive class separation. The second plot shows which attributes contribute the most to minimizing the within-class variances, highlighting the factors that help maintain compact and distinct clusters. These visualizations enable a deeper understanding of the model's decision-making process, making it easier to interpret and explain the results.

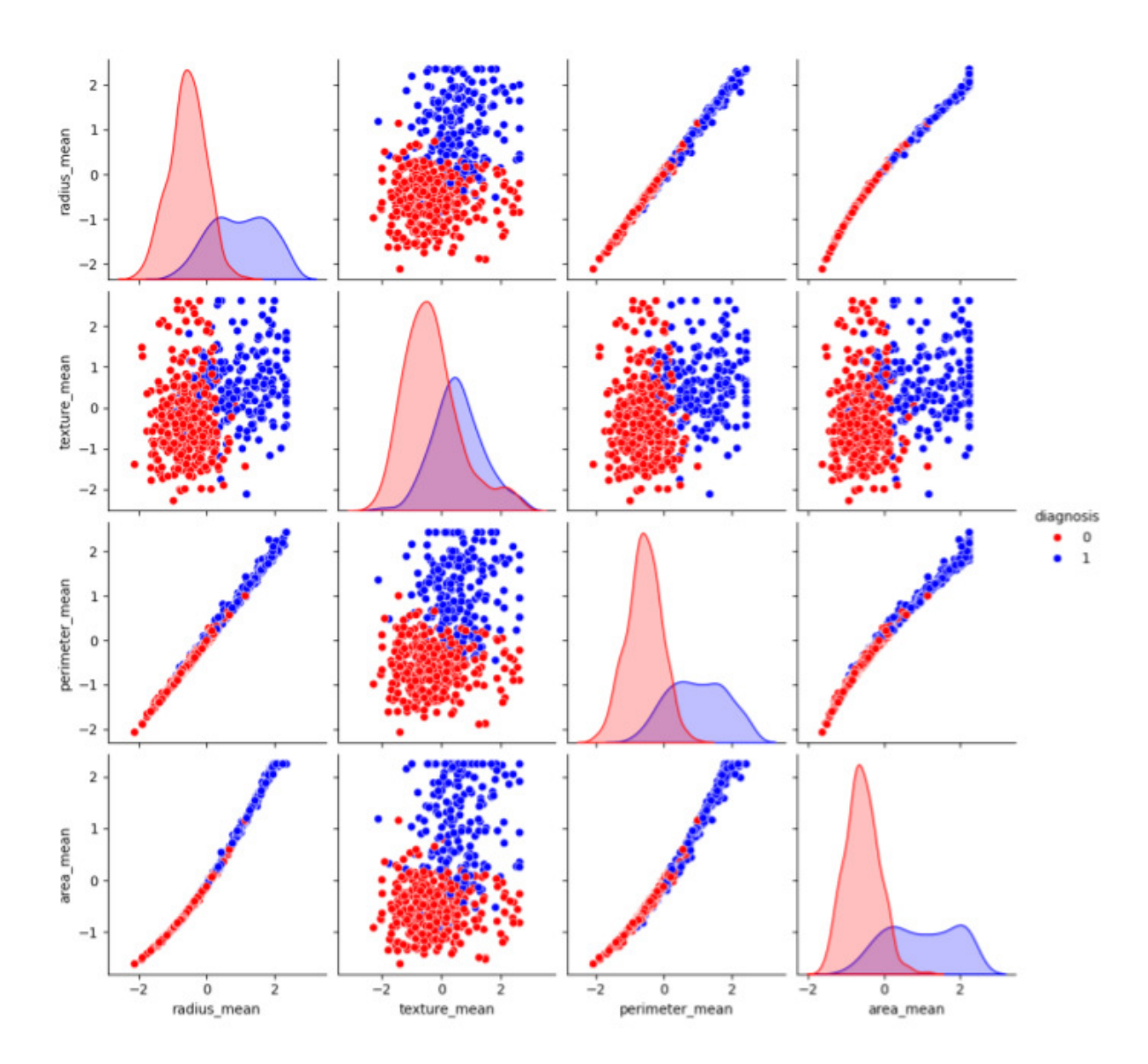


Figure 3: Pairplot of the first four predictor attributes in the WBCD dataset, colored by class labels. This pairplot presents only four of the 30 predictor attributes, projecting the 30-dimensional data into 1D and 2D spaces between individual attributes and attribute pairs. The visualizations show that these projections do not provide good separability between the two classes.

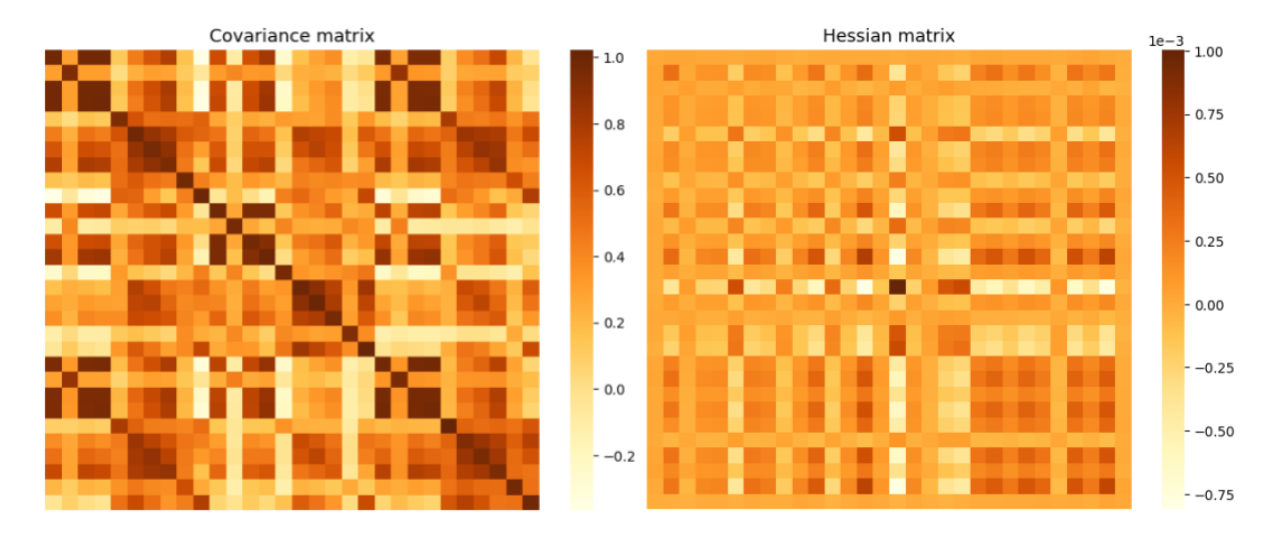


Figure 4: Heatmaps of the covariance matrix and the Hessian matrix for the WBCD dataset. The covariance matrix is computed unsupervisedly from the WBCD training set using Eq. 1. The Hessian matrix is evaluated on a deep learning model trained on the same training set using Eq. 3.

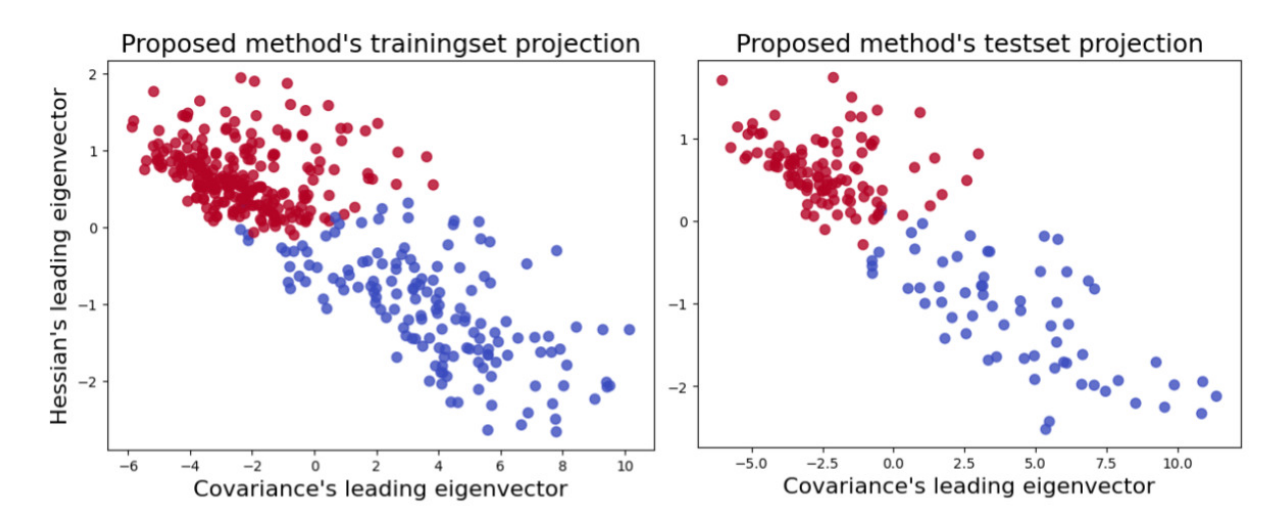


Figure 5: Training set and test set projections on the WBCD dataset using the proposed method. The proposed method projects the high-dimensional data into the leading eigendirections of the covariance and Hessian matrices. The training set projection illustrates how the training data is separated using the proposed method, while the test set projection shows the separation of new unseen data. Visually, the projections indicate good separability between the two classes, demonstrating the effectiveness of the proposed method.

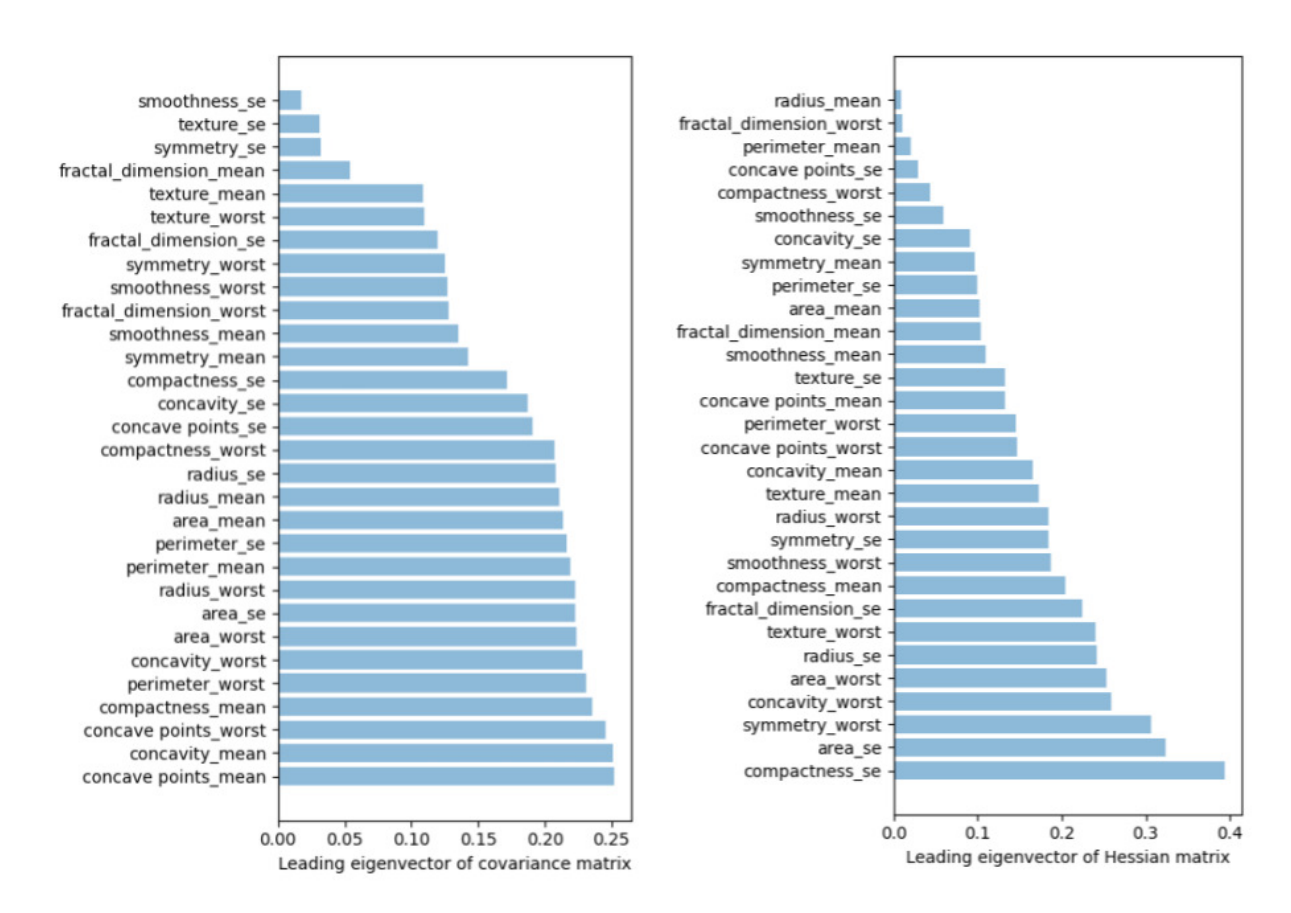


Figure 6: Parameter contributions to the leading eigenvectors of the covariance and Hessian matrices for the WBCD dataset. The contributions are calculated as the absolute values of the elements in the first eigenvector of the covariance and Hessian matrices, respectively. Parameters are sorted by their absolute contributions, and the horizontal bar plots display these sorted contributions for each parameter. The first plot indicates which attributes contribute the most to maximizing the between-class mean distance, while the second plot indicates which attributes contribute the most to minimizing the within-class variances.

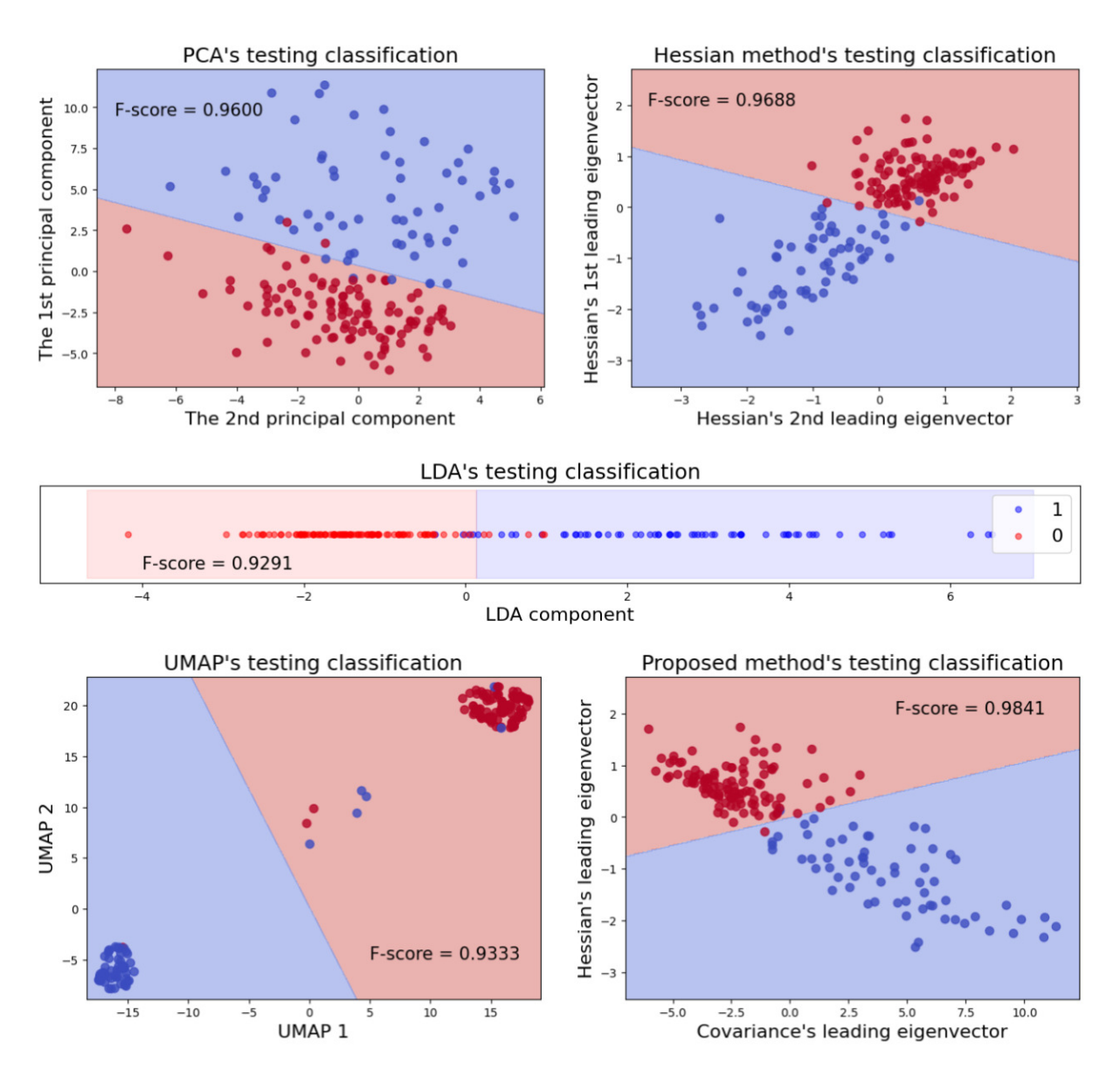


Figure 7: Training classification visualizations using various dimensionality reduction methods and linear SVM on the WBCD dataset. The plots show the separation of training data points using PCA, the Hessian method, LDA, UMAP, and the proposed method. Each subplot includes the separating SVM hyperplane and the corresponding F-score, indicating the classification performance of each method. UMAP achieves the highest performance with perfect separation, while the proposed method shows strong performance, surpassing the other methods.

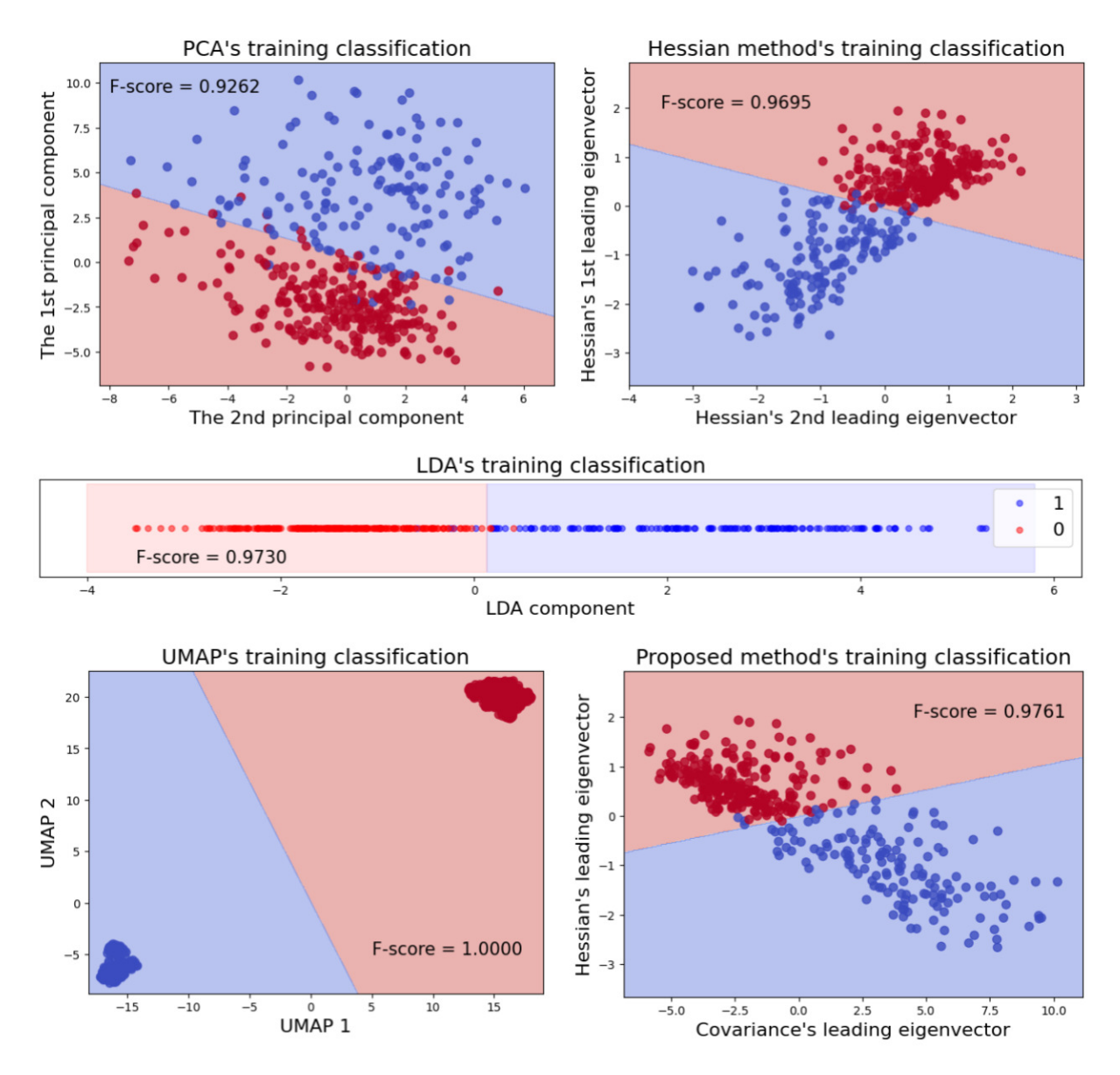


Figure 8: Testing classification visualizations using various dimensionality reduction methods and SVM on the WBCD dataset. The SVM hyperplanes trained on the training set projected using PCA, the Hessian method, LDA, UMAP, and the proposed method, as shown in Figure 7, are then applied to new unseen data points. The plots show the separation of these new data points. Each subplot includes the separating SVM hyperplane and the corresponding F-score, indicating the classification performance of each method on the test set. On new data, the proposed method outperforms all other methods, including UMAP, which had achieved the best performance on the training set. This demonstrates the superior generalization capability of the proposed method.

While Figures 5 illustrate the visual separations achieved by the proposed method, Figures 7 and 8 quantify their degrees of separation. These figures present the classification performance using various dimensionality reduction methods, including PCA, the Hessian method, LDA, UMAP, and the proposed method, evaluated with linear SVM on the WBCD dataset. Each subplot shows the separating SVM hyperplane along with the corresponding F-score, providing a quantitative measure of the classification performance. Figure 7 highlights the separation achieved on the training data, where UMAP achieves the highest performance with perfect separation, while the proposed method demonstrates strong performance, surpassing other methods. Figure 8 shows the performance on new unseen test data, where the proposed method outperforms all other methods, including UMAP, demonstrating its superior generalization capability.

7. Discussion

Our work offers a valuable theoretical perspective and a practical method, emphasizing the utility of simplicity in achieving noteworthy outcomes. We present a theoretical framework that elucidates a significant relationship between covariance and Hessian matrices. This framework, supported by our formal proof, connects covariance eigenanalysis with the first LDA criterion (the concept of separation) and Hessian eigenanalysis with the second (the concept of *compactness*). While this theoretical clarity is compelling, the effectiveness of our method, demonstrated across diverse datasets, is contingent upon relatively ideal conditions as outlined in Section 3. These conditions include assumptions about data isotropy, specifically the dataset subsets corresponding to each class being approximately isotropic around their respective means, and the dominance of leading eigenvalues, which are crucial for the method's success in practical applications.

The experiments conducted on the WBCD dataset illustrate these points. As shown in Figure 9, the absolute covariance matrices for each class in the WBCD dataset reveal a pattern that approximates the isotropic condition. The relatively uniform higher values along the diagonal and generally lower values in the off-diagonal elements indicate that the covariance matrices are nearly proportional to the identity matrix. As discussed in Section 3, the WBCD dataset being normalized (as

with the other datasets used in this study) helps approximate isotropy, as does the dataset being a good dataset with low redundancy among attributes. This near-isotropy supports the method's effectiveness in maximizing the between-class mean distance when projecting the WBCD data into the leading eigenvector of the covariance matrix, as suggested by Theorem 1.

Moreover, the eigenspectra displayed in Figure 10 highlight the dominance of the first eigenvalues in both the covariance and Hessian matrices. The eigenvalues are spread over several orders of magnitude on a logarithmic scale, often with approximately uniform spacing. Notably, the first eigenvalue for both matrices is situated on a different decade from the second and the subsequent eigenvalues indicating a significant separation in magnitude. This characteristic, especially pronounced in the Hessian matrix, is indicative of a "sloppy" model [53, 54, 55, 56, 57, 58, 59], where a few stiff directions dominate. Similarly, in the covariance matrix, this pattern suggests a dominant underlying structure or trend in the data. This distribution ensures that the leading eigenvector captures a significant portion of the variance or curvature, crucial for the proposed method's effectiveness in distinguishing between classes.

In contrast, datasets that do not fit the ideal conditions of isotropy and dominant leading eigenvalues may present challenges for the proposed method. For instance, if the covariance matrix elements are random or lack a pattern approximating proportionality to the identity matrix, which can occur in unnormalized datasets or datasets with high redundancy among attributes, the method's effectiveness may be compromised. Additionally, if the covariance and/or Hessian matrices exhibit relatively uniform eigenvalues, where the leading eigenvalues are not sufficiently dominant, the method may not perform as effectively.

In our experiments, the proposed method outperforms PCA and the Hessian method by comprehensively addressing both LDA criteria—maximizing between-class mean distance and minimizing within-class variances. Unlike PCA, which predominantly focuses on the former and lacks the guidance of class labels, our supervised approach considers both aspects. Despite the computational efficiency associated with unsupervised dimension reduction methods [72], our approach demonstrates the added value of incorporating class labels. This key insight also underlies our outperformance of KPCA,

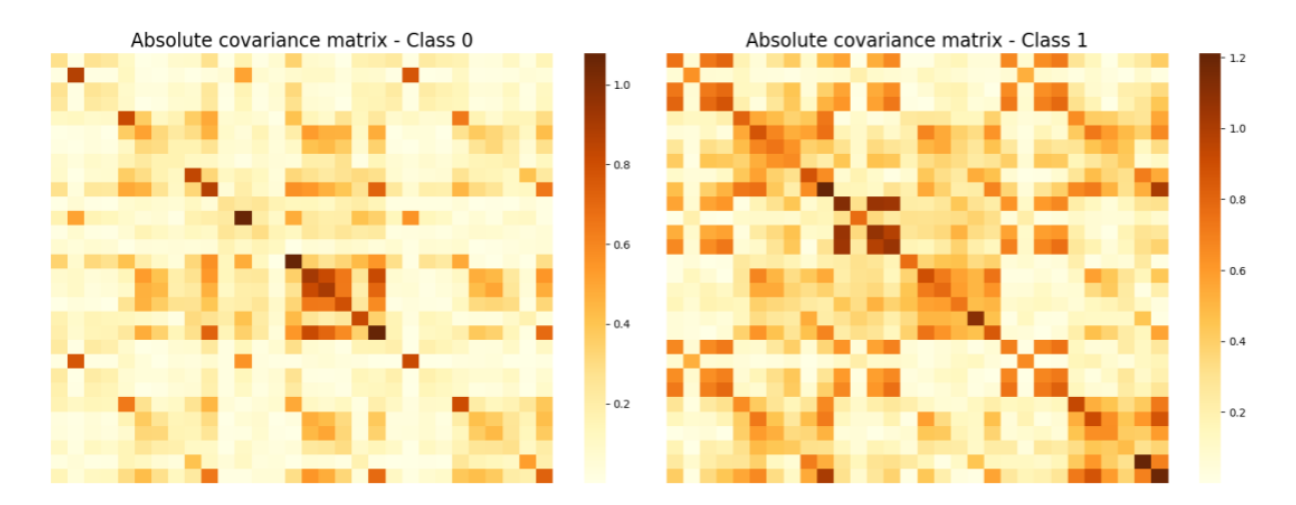


Figure 9: Absolute covariance matrices for WBCD dataset by class. The figure presents the absolute values of the covariance matrices for the WBCD dataset, calculated separately for each class. These matrices highlight the strength of linear relationships between features within each class. In these absolute covariance matrices, the approximate isotropic condition is evidenced by the relatively uniform higher values along the diagonal and the generally lower values in the off-diagonal elements. Specifically, for Class 0, the average diagonal value is 0.5655, and the average non-diagonal value is 0.1566; for Class 1, these values are 0.8503 and 0.2828, respectively. These characteristics, though not starkly isotropic, approximate the conditions where the covariance matrices are proportional to the identity matrix. This approximation helps ensure the applicability of Theorem 1 in higher dimensions.

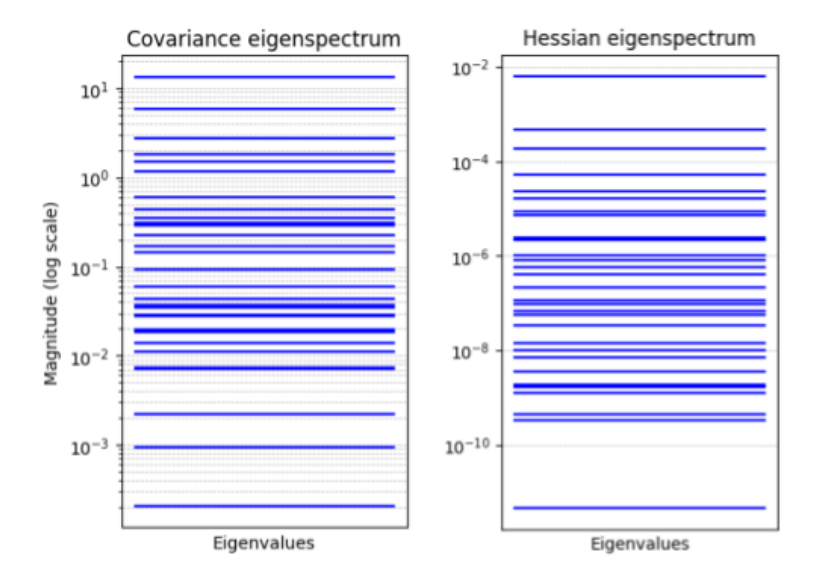


Figure 10: Eigenspectra of Covariance and Hessian Matrices for the WBCD Dataset. The plots display the eigenspectra of the covariance (left) and Hessian (right) matrices on a logarithmic scale. In both spectra, it is visible that the eigenvalues are spread over several orders of magnitude, often with approximately uniform spacing between them. Remarkably, the first eigenvalue in both matrices is positioned an order of magnitude above the second and subsequent eigenvalues, indicating a substantial difference in scale. This distribution suggests that the leading eigenvector captures a substantial portion of the variance or curvature, which is crucial for the effectiveness of the proposed method.

which, despite operating on non-linearities, remains essentially unsupervised in nature. While the Hessian method concentrates on minimizing within-class variances, our method optimally combines the strengths of PCA and the Hessian, effectively identifying feature space directions that enhance both between-class separation and within-class compactness.

While the proposed method employs the LDA criteria, it surpasses LDA itself in all cases. Figures 7 and 8 visually demonstrates the advantages of the proposed method over LDA. LDA is limited to a one-dimensional projection for binary classification problems [51], where it seeks to identify a single direction that simultaneously satisfies the two criteria. Conversely, the proposed method splits the task of meeting the criteria into two directions. The utilization of higher dimensionality in the proposed method increases the likelihood of discovering class separability, aligning with Cover's theorem [73]. KDA, operating on a non-linear mode, outperforms LDA in all cases, yet it remains fundamentally confined to one dimension, restricting its effectiveness in capturing intricate class-specific patterns compared to our proposed method.

Our method outperforms LOL by leveraging non-linear modes of operation, providing a distinct advantage in capturing complex patterns beyond the linear capabilities of LOL. UMAP exhibits good class separability with the widest margin as shown in Figures 7 and 8. However, it is important to note that UMAP is not inherently a classification technique, and thus, it fails to generalize well to new data in Figure 8 . Similar limitations apply to LLE, which, although effective in revealing local data structures, lacks the inherent capability for classification and generalization.

Figures 7 and 8 also underscores the simplicity and interpretability of linear SVMs as basic linear classifiers in dealing with low-dimensional data. The figure shows clear visualizations of the SVM's decision boundaries and separation achieved through the various dimensionality reduction methods. Notably, our proposed method combined with linear SVMs offers valuable insights into the decision-making process within the underlying DNN. Leveraging the transparency and interpretability provided by SVMs to address the inherent opacity of DNNs, our method bridges the gap between complex DNNs and comprehensible, highly accurate decision processes within a 2D space.

In another perspective, our proposed method

highlights the effective use of DNNs for data projection and representation. In this approach, DNNs serve as a classifier whose decision-making process can be encapsulated in the Hessian matrix. By extracting the leading eigenvector from this matrix, we capture significant classification information, which is then used as one of the key projection directions in our proposed method. This process leverages the deep learning model's ability to distill complex patterns into a compact and informative representation. This aligns with the findings of previous work, such as that by Hinton and Salakhutdinov [74], which highlights the potential of neural networks in enhancing data representation and separability.

The proposed method shows promising performance, but it has certain limitations. The applicability of our approach is based on the premise that a DNN model is already in place. Our method operates on top of the underlying DNN, so any short-comings or biases in the DNN's performance will naturally reflect in the results obtained from our approach. The limitation of our method lies in its dependence on the quality and accuracy of the underlying DNN.

Another limitation of the proposed method arises from its reliance on relatively ideal dataset conditions for optimal performance. In practical applications, not all datasets will meet these criteria. For instance, datasets with high redundancy among attributes, lacking proper normalization, or involving models that are not sufficiently sloppy may not exhibit the desired isotropy or dominance of leading eigenvalues. In such cases, the method's performance may degrade, potentially limiting its applicability to a broader range of datasets.

An important trajectory for future work involves investigating the extension of our methodology to accommodate various loss functions beyond binary cross-entropy. The mathematical derivation in our current work relies on the elegant relationship between binary cross-entropy loss and within-class variances. Even though the binary cross-entropy loss function is widely recognized as the standard loss function for binary classification models [75], exploring the adaptability of our method to different loss functions will contribute to a more comprehensive understanding of the method's versatility, but requires careful scrutiny to establish analogous connections.

Simultaneously, we recognize the need to extend our methodology from binary to multiclass classification. The binary classification focus in this work stems from foundational aspects guiding our formal proof, which is designed around binary assumptions to facilitate a streamlined and elegant derivation process. In particular, the use of binary cross-entropy as the loss function and the utilization of a linear SVM for evaluation inherently adhere to binary classification. Moving forward, careful exploration is needed to adapt our approach to multiclass scenarios to ensure its applicability and effectiveness across a broader range of classification tasks.

It is also important to validate our method on more complex and modern datasets. In this regard, another promising direction for future work is the application of our method to classification problems involving image datasets [76, 77, 78, 79, 80, 81, 82, 83, 84], audio datasets [85, 86, 87, 88, 89, 90], and their integration with additional features such as patient information or demographic data [91, 92]. Leveraging datasets that involve more intricate patterns and higher-dimensional data will be instrumental in demonstrating the full potential and scalability of our methodology.

8. Conclusion

In this paper, we have made several contributions to the fields of binary classification and dimensionality reduction:

- Theoretical insight: We provide a formal framework linking the eigenanalysis of covariance and Hessian matrices to LDA criteria, which enhances the understanding of class separability.
- Novel method: We propose a method that integrates covariance and Hessian matrices for dimensionality reduction, aimed at improving class separability in binary classification tasks.
- Data conditions: We define certain ideal dataset conditions under which our method performs optimally, ensuring that the theoretical assumptions are met and maximizing the method's effectiveness in practical applications.
- Empirical validation: Our method, tested across various datasets, generally outperforms existing techniques, highlighting its potential robustness and effectiveness under the right conditions.

- **Practical utility**: The method retains a computational complexity comparable to traditional approaches, suggesting its practicality in real-world applications.
- Improved explainability: By integrating our method with linear SVMs, we enhance the explainability and interpretability of deep neural networks, addressing their typical opacity and facilitating better understanding of their decision-making processes.

9. Reproducibility statement

The detailed proofs for the theoretical foundations, emphasizing the maximization of betweenclass mean distance and minimization of withinclass variance, are provided in Appendix A. The complete source code and datasets for our experiments are accessible through the following links:

- 1. WBCD dataset experiment: Link to Colab notebook
- 2. Heart disease dataset experiment: Link to Colab notebook
- 3. Neural spike train dataset experiment: Link to Colab notebook
- 4. Pima Indians diabetes dataset experiment: Link to Colab notebook
- 5. Illustrative case study on WBCD dataset: Link to Colab notebook

These notebooks contain the complete source code along with the datasets accessed from the same Google Drive account, facilitating easy reproduction and comprehension of our results.

10. Acknowledgments

This research is supported by the European Union's Horizon 2020 research and innovation programme under grant agreement Sano No 857533 and the project of the Minister of Science and Higher Education "Support for the activity of Centers of Excellence established in Poland under Horizon 2020" on the basis of the contract number MEiN/2023/DIR/3796.

References

- T.-H. Nagai, The covariance matrix of green's functions and its application to machine learning, ArXiv abs/2004.06481 (2020).
- [2] H. Q. Minh, V. Murino, Covariances in computer vision and machine learning, in: Covariances in Computer Vision and Machine Learning, 2017.
- [3] G. Serra, C. Grana, M. Manfredi, R. Cucchiara, Covariance of covariance features for image classification, Proceedings of International Conference on Multimedia Retrieval (2014).
- [4] K. Lenc, A. Vedaldi, Learning covariant feature detectors, in: ECCV Workshops, 2016.
- [5] P. D. Hoff, X. Niu, A covariance regression model, Statistica Sinica 22 (2011) 729–753.
- [6] B.-C. Kuo, D. A. Landgrebe, A covariance estimator for small sample size classification problems and its application to feature extraction, IEEE Trans. Geosci. Remote. Sens. 40 (2002) 814–819.
- [7] C. Lam, High-dimensional covariance matrix estimation, Wiley Interdisciplinary Reviews: Computational Statistics 12 (2019).
- [8] A. Dawid, P. Huembeli, M. Tomza, M. Lewenstein, A. Dauphin, Hessian-based toolbox for reliable and interpretable machine learning in physics, Machine Learning: Science and Technology 3 (2021).
- [9] S. Fu, W. Liu, D. Tao, Y. Zhou, L. Nie, Hesgcn: Hessian graph convolutional networks for semi-supervised classification, Inf. Sci. 514 (2020) 484–498.
- [10] Z. Yao, A. Gholami, K. Keutzer, M. W. Mahoney, Pyhessian: Neural networks through the lens of the hessian, 2020 IEEE International Conference on Big Data (Big Data) (2019) 581–590.
- [11] G. Krishnasamy, R. Paramesran, Hessian semisupervised extreme learning machine, Neurocomputing 207 (2016) 560–567.
- [12] S. Wiesler, J. Li, J. Xue, Investigations on hessian-free optimization for cross-entropy training of deep neural networks, in: Interspeech, 2013.
- [13] R. H. Byrd, G. M. Chin, W. Neveitt, J. Nocedal, On the use of stochastic hessian information in optimization methods for machine learning, SIAM J. Optim. 21 (2011) 977–995.
- [14] J. Martens, Deep learning via hessian-free optimization, in: International Conference on Machine Learning, 2010.
- [15] O. M. Shir, A. Yehudayoff, On the covariance-hessian relation in evolution strategies, Theoretical Computer Science 801 (2020) 157–174.
- [16] R. A. Fisher, The use of multiple measurements in taxonomic problems, Annals of eugenics 7 (2) (1936) 179– 188.
- [17] P. Xanthopoulos, P. M. Pardalos, T. B. Trafalis, P. Xanthopoulos, P. M. Pardalos, T. B. Trafalis, Linear discriminant analysis, Robust data mining (2013) 27–33.
- [18] A. Sharma, S. Imoto, S. Miyano, A between-class overlapping filter-based method for transcriptome data analysis, Journal of bioinformatics and computational biology 10 (05) (2012) 1250010.
- [19] A. Sharma, K. K. Paliwal, Cancer classification by gradient lda technique using microarray gene expression data, Data & Knowledge Engineering 66 (2) (2008) 338– 347.
- [20] B. Moghaddam, Y. Weiss, S. Avidan, Generalized spec-

- tral bounds for sparse lda, in: Proceedings of the 23rd international conference on Machine learning, 2006, pp. 641-648.
- [21] S. Dudoit, J. Fridlyand, T. P. Speed, Comparison of discrimination methods for the classification of tumors using gene expression data, Journal of the American statistical association 97 (457) (2002) 77–87.
- [22] H.-P. Chan, D. Wei, M. A. Helvie, B. Sahiner, D. D. Adler, M. M. Goodsitt, N. Petrick, Computer-aided classification of mammographic masses and normal tissue: linear discriminant analysis in texture feature space, Physics in Medicine & Biology 40 (5) (1995) 857.
- [23] A. Tharwat, T. Gaber, A. E. Hassanien, Onedimensional vs. two-dimensional based features: Plant identification approach, Journal of Applied logic 24 (2017) 15–31.
- [24] T. Gaber, A. Tharwat, V. Snasel, A. E. Hassanien, Plant identification: Two dimensional-based vs. one dimensional-based feature extraction methods, in: 10th international conference on soft computing models in industrial and environmental applications, Springer, 2015, pp. 375–385.
- [25] S. Rezzi, D. E. Axelson, K. Héberger, F. Reniero, C. Mariani, C. Guillou, Classification of olive oils using high throughput flow 1h nmr fingerprinting with principal component analysis, linear discriminant analysis and probabilistic neural networks, Analytica Chimica Acta 552 (1-2) (2005) 13–24.
- [26] K. Héberger, E. Csomós, L. Simon-Sarkadi, Principal component and linear discriminant analyses of free amino acids and biogenic amines in hungarian wines, Journal of agricultural and food chemistry 51 (27) (2003) 8055–8060.
- [27] L. Chen, N. C. Carpita, W.-D. Reiter, R. H. Wilson, C. Jeffries, M. C. McCann, A rapid method to screen for cell-wall mutants using discriminant analysis of fourier transform infrared spectra, The Plant Journal 16 (3) (1998) 385–392.
- [28] K. K. Paliwal, A. Sharma, Improved pseudoinverse linear discriminant analysis method for dimensionality reduction, International Journal of Pattern Recognition and Artificial Intelligence 26 (01) (2012) 1250002.
- [29] L. Yuan, Z.-c. Mu, Ear recognition based on 2d images, in: 2007 First IEEE International Conference on Biometrics: Theory, Applications, and Systems, IEEE, 2007, pp. 1–5.
- [30] C. H. Park, H. Park, Fingerprint classification using fast fourier transform and nonlinear discriminant analysis, Pattern Recognition 38 (4) (2005) 495–503.
- [31] X. Wang, X. Tang, Random sampling Ida for face recognition, in: Proceedings of the 2004 IEEE Computer Society Conference on Computer Vision and Pattern Recognition, 2004. CVPR 2004., Vol. 2, IEEE, 2004, pp. II–II.
- [32] H. Yu, J. Yang, A direct lda algorithm for highdimensional data—with application to face recognition, Pattern recognition 34 (10) (2001) 2067–2070.
- [33] L.-F. Chen, H.-Y. M. Liao, M.-T. Ko, J.-C. Lin, G.-J. Yu, A new lda-based face recognition system which can solve the small sample size problem, Pattern recognition 33 (10) (2000) 1713–1726.
- [34] R. Haeb-Umbach, H. Ney, Linear discriminant analysis for improved large vocabulary continuous speech recognition., in: icassp, Vol. 92, Citeseer, 1992, pp. 13–16.
- [35] S. Lloyd, Least squares quantization in pcm, IEEE

- transactions on information theory 28 (2) (1982) 129–137.
- [36] E. W. Forgy, Cluster analysis of multivariate data: efficiency versus interpretability of classifications, biometrics 21 (1965) 768–769.
- [37] L. Kaufman, Partitioning around medoids (program pam), Finding groups in data 344 (1990) 68–125.
- [38] L. Kaufman, P. J. Rousseeuw, Finding groups in data: an introduction to cluster analysis, John Wiley & Sons, 2009.
- [39] S. C. Johnson, Hierarchical clustering schemes, Psychometrika 32 (3) (1967) 241–254.
- [40] T. Zhang, R. Ramakrishnan, M. Livny, Birch: an efficient data clustering method for very large databases, ACM sigmod record 25 (2) (1996) 103–114.
- [41] P. H. Andrews, R. R. Sokal, Numerical taxonomy: The principles and practice of numerical classification, WH Freeman, 1973.
- [42] R. Hidalgo, A. DeVito, N. Salah, A. S. Varde, R. W. Meredith, Inferring phylogenetic relationships using the smith-waterman algorithm and hierarchical clustering, in: 2022 IEEE International Conference on Big Data (Big Data), IEEE, 2022, pp. 5910–5914.
- [43] M. Ester, H.-P. Kriegel, J. Sander, X. Xu, et al., A density-based algorithm for discovering clusters in large spatial databases with noise, in: kdd, Vol. 96, 1996, pp. 226–231.
- [44] R. J. Campello, D. Moulavi, J. Sander, Density-based clustering based on hierarchical density estimates, in: Pacific-Asia conference on knowledge discovery and data mining, Springer, 2013, pp. 160–172.
- [45] M. Ankerst, M. M. Breunig, H.-P. Kriegel, J. Sander, Optics: Ordering points to identify the clustering structure, ACM Sigmod record 28 (2) (1999) 49–60.
- [46] R. Agrawal, J. Gehrke, D. Gunopulos, P. Raghavan, Automatic subspace clustering of high dimensional data for data mining applications, in: Proceedings of the 1998 ACM SIGMOD international conference on Management of data, 1998, pp. 94–105.
- [47] W. I. D. Mining, Data mining: Concepts and techniques, Morgan Kaufinann 10 (559-569) (2006) 4.
- [48] W. I. D. Mining, Introduction to data mining, Springer, 2006.
- [49] Y. Zhao, G. Karypis, Evaluation of hierarchical clustering algorithms for document datasets, in: Proceedings of the eleventh international conference on Information and knowledge management, 2002, pp. 515–524.
- [50] Y. Liu, Z. Li, H. Xiong, X. Gao, J. Wu, Understanding of internal clustering validation measures, in: 2010 IEEE international conference on data mining, Ieee, 2010, pp. 911–916.
- [51] J. Ye, R. Janardan, Q. Li, Two-dimensional linear discriminant analysis, Advances in neural information processing systems 17 (2004).
- [52] E. Barshan, M.-E. Brunet, G. K. Dziugaite, Relatif: Identifying explanatory training samples via relative influence, in: International Conference on Artificial Intelligence and Statistics, PMLR, 2020, pp. 1899–1909.
- [53] J. J. Waterfall, F. P. Casey, R. N. Gutenkunst, K. S. Brown, C. R. Myers, P. W. Brouwer, V. Elser, J. P. Sethna, Sloppy-model universality class and the vandermonde matrix, Physical review letters 97 (15) (2006) 150601.
- [54] M. K. Transtrum, B. B. Machta, J. P. Sethna, Why are nonlinear fits to data so challenging?, Physical review

- letters 104 (6) (2010) 060201.
- [55] M. K. Transtrum, B. B. Machta, J. P. Sethna, Geometry of nonlinear least squares with applications to sloppy models and optimization, Physical Review E—Statistical, Nonlinear, and Soft Matter Physics 83 (3) (2011) 036701.
- [56] M. K. Transtrum, B. B. Machta, K. S. Brown, B. C. Daniels, C. R. Myers, J. P. Sethna, Perspective: Sloppiness and emergent theories in physics, biology, and beyond, The Journal of chemical physics 143 (1) (2015).
- [57] B. B. Machta, R. Chachra, M. K. Transtrum, J. P. Sethna, Parameter space compression underlies emergent theories and predictive models, Science 342 (6158) (2013) 604–607.
- [58] D. V. Raman, J. Anderson, A. Papachristodoulou, Delineating parameter unidentifiabilities in complex models, Physical Review E 95 (3) (2017) 032314.
- [59] A. Hartoyo, P. J. Cadusch, D. T. Liley, D. G. Hicks, Parameter estimation and identifiability in a neural population model for electro-cortical activity, PLoS computational biology 15 (5) (2019) e1006694.
- [60] B. Schölkopf, A. Smola, K.-R. Müller, Kernel principal component analysis, in: International conference on artificial neural networks, Springer, 1997, pp. 583–588.
- [61] L. McInnes, J. Healy, J. Melville, Umap: Uniform manifold approximation and projection for dimension reduction, arXiv preprint arXiv:1802.03426 (2018).
- [62] S. T. Roweis, L. K. Saul, Nonlinear dimensionality reduction by locally linear embedding, science 290 (5500) (2000) 2323–2326.
- [63] J. T. Vogelstein, E. W. Bridgeford, M. Tang, D. Zheng, C. Douville, R. Burns, M. Maggioni, Supervised dimensionality reduction for big data, Nature communications 12 (1) (2021) 2872.
- [64] S. Mika, G. Ratsch, J. Weston, B. Scholkopf, K.-R. Mullers, Fisher discriminant analysis with kernels, in: Neural networks for signal processing IX: Proceedings of the 1999 IEEE signal processing society workshop (cat. no. 98th8468), Ieee, 1999, pp. 41–48.
- [65] W. N. Street, W. H. Wolberg, O. L. Mangasarian, Nuclear feature extraction for breast tumor diagnosis, in: Biomedical image processing and biomedical visualization, Vol. 1905, SPIE, 1993, pp. 861–870.
- [66] R. Detrano, A. Janosi, W. Steinbrunn, M. Pfisterer, J.-J. Schmid, S. Sandhu, K. H. Guppy, S. Lee, V. Froelicher, International application of a new probability algorithm for the diagnosis of coronary artery disease, The American journal of cardiology 64 (5) (1989) 304–310.
- [67] J. W. Smith, J. E. Everhart, W. Dickson, W. C. Knowler, R. S. Johannes, Using the adap learning algorithm to forecast the onset of diabetes mellitus, in: Proceedings of the annual symposium on computer application in medical care, American Medical Informatics Association, 1988, p. 261.
- [68] D. Tsai, E. John, T. Chari, R. Yuste, K. Shepard, High-channel-count, high-density microelectrode array for closed-loop investigation of neuronal networks, in: 2015 37th Annual International Conference of the IEEE Engineering in Medicine and Biology Society (EMBC), IEEE, 2015, pp. 7510–7513.
- [69] M. O. Heuschkel, M. Fejtl, M. Raggenbass, D. Bertrand, P. Renaud, A three-dimensional multi-electrode array for multi-site stimulation and recording in acute brain slices, Journal of neuroscience methods 114 (2) (2002)

- 135 148.
- [70] I. Lazarevich, I. Prokin, B. Gutkin, V. Kazantsev, Spikebench: An open benchmark for spike train time-series classification, PLOS Computational Biology 19 (1) (2023) e1010792.
- [71] M. Christ, N. Braun, J. Neuffer, A. W. Kempa-Liehr, Time series feature extraction on basis of scalable hypothesis tests (tsfresh-a python package), Neurocomputing 307 (2018) 72-77.
- [72] C. Shen, M. Sun, M. Tang, C. E. Priebe, Generalized canonical correlation analysis for classification, Journal of Multivariate Analysis 130 (2014) 310–322.
- [73] T. M. Cover, Geometrical and statistical properties of systems of linear inequalities with applications in pattern recognition, IEEE transactions on electronic computers (3) (1965) 326–334.
- [74] G. E. Hinton, R. R. Salakhutdinov, Reducing the dimensionality of data with neural networks, science 313 (5786) (2006) 504–507.
- [75] Y. Wang, L. Liu, T. Huang, Detection of image tampering using multiscale fusion and anomalousness assessment, Image Processing, Electronics and Applications (2024).
- [76] H. Al Abboodi, A. Al-funjan, N. Hamza, A lightweight deep learning-based ocular disease prediction model using squeeze-and-excitation network architecture with mobilenet feature extraction, Journal of Intelligent Systems (2024).
- [77] P. Decoodt, D. Sierra-Sosa, L. Anghel, G. Cuminetti, Transfer learning video classification of preserved, midrange, and reduced left ventricular ejection fraction in echocardiography, Diagnostics (2024).
- [78] E. Vaghefi, S. An, M. McConnell, Exploration of retinal images for rapid classification of cardiovascular-kidneymetabolic (ckm) syndrome, Investigative Ophthalmology & Visual Science (2024).
- [79] S. Madhusudhan, D. Parry, Z. Gao, Detection of coexisting macular pathology in patients on hydroxychloroquine therapy using a foundation model, Investigative Ophthalmology & Visual Science (2024).
- [80] R. Salowe, S. Li, R. Lee, G. Ying, I. Lee, Utilizing deep learning to diagnose glaucoma from fundus photography in african ancestry individuals, Investigative Ophthalmology & Visual Science (2024).
- [81] O. Rainio, J. Tamminen, M. Venäläinen, Comparison of thresholds for a convolutional neural network classifying medical images, International Journal of Data Science and Analytics (2024).
- [82] P. Naik, K. Shraddha, S. Gowda, K. Theju, Herbid-a medicinal plant identification and recommendation model using machine learning algorithms, AIP Conference Proceedings (2024).
- [83] P. Kadam, S. Kadam, R. Bidwe, N. Shinde, Smart yoga: Machine learning approaches for real-time pose recognition and feedback, International Journal of Computing and Digital Systems (2024).
- [84] X. Yang, X. Guan, X. Meng, Dbformer: a deep learning model to predict tumor mutation burden of lung adenocarcinoma, in: International Symposium on Computer Architecture, SPIE, 2024.
- [85] B. Downward, J. Nordby, The aerosonicdb (ypad-0523) dataset for acoustic detection and classification of aircraft, arXiv preprint arXiv:2311.06368 (2023).
- [86] H. Bannour, K. Kancherlai, Z. Zhu, Optimizing audio advertising campaign delivery with a limited budget,

- in: 2023 International Conference on Machine Learning and Applications (ICMLA), IEEE, 2023.
- [87] V. Narayanan, M. Hemalatha, Bioacoustic estimation of avian vocalizations for capuchin bird density in forests, in: 2024 IEEE International Conference on Acoustics, Speech and Signal Processing (ICASSP), IEEE, 2024.
- [88] J. Cai, Y. Song, J. Wu, X. Chen, Unveiling dysphonia: Voice disorder classification with stacking ensemble learning method utilizing mfcc, SSRN (2024).
- [89] A. Navine, T. Denton, M. Weldy, P. Hart, All thresholds barred: direct estimation of call density in bioacoustic data, Frontiers in Bird Science (2024).
- [90] S. Huddart, V. Yadav, S. K. Sieberts, L. Omberg, M. Raberahona, R. Rakotoarivelo, I. N. Lyimo, O. Lweno, D. J. Christopher, N. V. Nhung, et al., Solicited cough sound analysis for tuberculosis triage testing: The coda tb dream challenge dataset, medRxiv (2024).
- [91] J. Yadav, A. S. Varde, L. Xie, Comprehensive cough data analysis on coda tb, in: 2023 IEEE International Conference on Big Data (BigData), IEEE, 2023, pp. 6311–6313.
- [92] A. Kodipalli, S. Fernandes, S. Das, Evaluation of a novel ensemble deep neural network model and explainable ai for accurate segmentation and classification of ovarian tumors using ct images, Diagnostics (2024).

Appendix A. Full proofs: maximizing the squared between-class mean distance and minimizing the within-class variance

Appendix A.1. Proof of Theorem 1 - Maximizing Covariance for Maximizing Squared Between-Class Mean Distance

To prove that maximizing the variance will maximize the squared between-class mean distance, we start by considering two sets of 1D data points representing two classes, denoted as C_1 and C_2 , each consisting of n samples. The data in C_1 and C_2 follow the same underlying distribution centered around their respective means, m_1 and m_2 . In other words, C_2 can be understood as a reflection of C_1 with the axis of reflection positioned at the overall mean, denoted as m, effectively giving rise to a shifted configuration. Specifically, the indices for C_1 range from 1 to n, while the indices for C_2 range from n+1 to 2n.

For any pair of data points x_i and x_j , where $1 \le i \le n$ and $n+1 \le j \le 2n$, the difference between x_i and m_1 is equal to the difference between x_j and m_2 , i.e., $x_i - m_1 = x_j - m_2$. This relationship ensures that the shifted copies of C_1 and C_2 maintain the same relative distances from their respective means, preserving the identical distribution in both sets. Furthermore, the variances of C_1 and C_2 , are equal, denoted as $\sigma_1^2 = \sigma_2^2 = \sigma_w^2$, and the combined data from C_1 and C_2 has a variance of σ^2 .

The between-class mean distance, denoted as d, represents the separation between the means of C_1 and C_2 . We can express the means as $m_1 = m - \frac{d}{2}$ and $m_2 = m + \frac{d}{2}$, where m is effectively located in the middle, equidistant from both m_1 and m_2 .

The variance of the combined data is given by:

$$\sigma^2 = \frac{1}{2n-1} \left(\sum_{i=1}^n (x_i - m)^2 + \sum_{i=n+1}^{2n} (x_i - m)^2 \right)$$

To simplify the expression, we substitute $m = m_1 + \frac{1}{2}d$ and $m = m_2 - \frac{1}{2}d$. This yields:

$$s^{2} = \frac{1}{2n-1} \left(\sum_{i=1}^{n} \left(x_{i} - \left(m_{1} + \frac{1}{2} d \right) \right)^{2} + \sum_{i=n+1}^{2n} \left(x_{i} - \left(m_{2} - \frac{1}{2} d \right) \right)^{2} \right)$$

$$= \frac{1}{2n-1} \left(\sum_{i=1}^{n} \left((x_{i} - m_{1}) - \frac{1}{2} d \right)^{2} + \sum_{i=n+1}^{2n} \left((x_{i} - m_{2}) + \frac{1}{2} d \right)^{2} \right)$$

$$= \frac{1}{2n-1} \left(\sum_{i=1}^{n} \left((x_{i} - m_{1})^{2} - (x_{i} - m_{1}) d + \frac{1}{4} d^{2} \right) \right)$$

$$+ \sum_{i=n+1}^{2n} \left((x_{i} - m_{2})^{2} + (x_{i} - m_{2}) d + \frac{1}{4} d^{2} \right) \right)$$

$$= \frac{1}{2n-1} \left(\sum_{i=1}^{n} \left((x_{i} - m_{1})^{2} + \frac{1}{4} d^{2} \right) - \sum_{i=1}^{n} \left((x_{i} - m_{2}) d \right)$$

$$+ \sum_{i=n+1}^{2n} \left((x_{i} - m_{2})^{2} + \frac{1}{4} d^{2} \right) \right) + \sum_{i=n+1}^{2n} \left((x_{i} - m_{2})^{2} + \frac{1}{4} d^{2} \right) \right)$$

$$+ \sum_{i=n+1}^{2n} \left((x_{i} - m_{2}) d \right) - \sum_{i=1}^{n} \left((x_{i} - m_{1}) d \right)$$

$$= \frac{1}{2n-1} \left(\sum_{i=1}^{n} \left((x_{i} - m_{1})^{2} + \frac{1}{4} d^{2} \right) + \sum_{i=n+1}^{2n} \left((x_{i} - m_{2})^{2} + \frac{1}{4} d^{2} \right) \right) \right)$$

$$+ \left(\sum_{i=n+1}^{2n} \left((x_{i} - m_{2}) - \sum_{i=1}^{n} \left((x_{i} - m_{1}) d \right) d$$

The property of the identical distribution in both sets suggests $\sum_{i=n+1}^{2n} (x_i - m_2) - \sum_{i=1}^{n} (x_i - m_1) = 0$. So, we get:

$$\sigma^{2} = \frac{1}{2n-1} \left(\sum_{i=1}^{n} \left((x_{i} - m_{1})^{2} + \frac{1}{4} d^{2} \right) + \sum_{i=n+1}^{2n} \left((x_{i} - m_{2})^{2} + \frac{1}{4} d^{2} \right) \right)$$

$$= \frac{1}{2n-1} \left(\sum_{i=1}^{n} (x_{i} - m_{1})^{2} + \sum_{i=n+1}^{2n} (x_{i} - m_{2})^{2} + \frac{1}{2} n \cdot d^{2} \right)$$

$$\approx \frac{1}{2(n-1)} \left(\sum_{i=1}^{n} (x_{i} - m_{1})^{2} + \sum_{i=n+1}^{2n} (x_{i} - m_{2})^{2} \right) + \frac{1}{4} d^{2}$$

$$= \frac{1}{2} \left(\frac{\sum_{i=1}^{n} (x_{i} - m_{1})^{2}}{(n-1)} + \frac{\sum_{i=n+1}^{2n} (x_{i} - m_{2})^{2}}{(n-1)} \right) + \frac{1}{4} d^{2}$$

$$= \frac{1}{2} \left(\sigma_{w}^{2} + \sigma_{w}^{2} \right) + \frac{1}{4} d^{2}$$

$$= \sigma_{w}^{2} + \frac{1}{4} d^{2}.$$

Now, considering the data points representing the projected data onto an (Eigen)vector, we can utilize

the Variance Ratio Preservation Theorem for Projection onto a Vector, which establishes the relationship between σ^2 and σ_w^2 as follows:

$$\sigma_w^2 = \lambda \cdot \sigma^2$$

where λ is a constant between 0 and 1, determined by the distribution of the original data being projected. Substituting this equation into the previous expression, we have:

$$\sigma^2 = \lambda \cdot \sigma^2 + \frac{1}{4}d^2.$$

Let's rearrange the equation by moving $2\lambda \cdot \sigma^2$ to the left side:

$$\sigma^2 - \lambda \cdot \sigma^2 = \frac{1}{4}d^2.$$

Combining like terms:

$$(1 - \lambda) \cdot \sigma^2 = \frac{1}{4}d^2.$$

To solve for σ^2 , divide both sides by $(1 - \lambda)$:

$$\sigma^2 = \frac{\frac{1}{4}d^2}{1-\lambda} = \frac{r^2}{1-\lambda}$$

where $r = \frac{1}{2}d = m - m_1 = m_2 - m$.

We observe that the sign of σ^2 and d^2 will be the same since the denominator $1 - \lambda$ is always positive (as $0 < \lambda < 1$). Therefore, σ^2 is linearly proportional to d^2 .

Hence, maximizing the variance (σ^2) will maximize the squared between-class mean distance (d^2) as desired.

Appendix A.2. Proof of Theorem 2 - Maximizing Hessian for Minimizing Within-Class Variance

We aim to prove that maximizing the Hessian will minimize the within-class variance. Let θ denote a parameter of the classifier.

We define the within-class variance as the variance of a posterior distribution $p_{\theta}(\theta \mid c_i)$, which represents the distribution of the parameter θ given a class c_i . We denote the variance of this posterior distribution as σ_{post}^2 .

Recall that our Hessian is given by:

$$\mathbf{H}_{\theta} = -\left[\nabla_{\theta}^{2} \log p_{\theta}(c_{i} \mid \theta)\right]$$

However, according to [52], we can approximate the Hessian using Fisher information:

$$H_{\theta} \approx \mathbb{E}_{p_{\theta}} \left[\left(\nabla_{\theta} \log p_{\theta}(c_i \mid \theta) \right)^2 \right]$$

Assuming that a known normal distribution underlies the likelihood $p_{\theta}(c_i \mid \theta)$, i.e.,

$$p_{\theta}(c_i \mid \theta) = \frac{1}{\sqrt{2\pi\sigma^2}} \exp\left(-\frac{(\theta - \mu)^2}{2\sigma^2}\right)$$

where μ and σ are known constants, we can compute the Hessian as follows:

$$H_{\theta} = \mathbb{E}_{p_{\theta}} \left[\left(\nabla_{\theta} \log \frac{1}{\sqrt{2\pi\sigma^2}} \exp\left(-\frac{(\theta - \mu)^2}{2\sigma^2} \right) \right)^2 \right]$$

$$= \mathbb{E}_{p_{\theta}} \left[\left(\frac{\theta - \mu}{\sigma^2} \right)^2 \right]$$

$$= \frac{1}{\sigma^4} \mathbb{E}_{p_{\theta}} \left[(\theta - \mu)^2 \right]$$

$$= \frac{1}{\sigma^4} \sigma^2$$

$$= \frac{1}{\sigma^2}$$

Now, let us assume that the evidence $p(c_i)$ is a known constant ρ . We also assume that the prior distribution $p(\theta)$ follows a uniform distribution within the plausible range of θ , which is bounded by a known minimum value θ_{\min} and maximum value θ_{\max} . Formally:

$$p_{\theta}(\theta) = \begin{cases} \frac{1}{\theta_{\text{max}} - \theta_{\text{min}}}, & \text{if } \theta_{\text{min}} \leq \theta \leq \theta_{\text{max}} \\ 0, & \text{otherwise} \end{cases}$$

Based on Bayes' formula and the given assumptions, the posterior distribution within the plausible range of θ is:

$$p_{\theta}(\theta \mid c_i) = \frac{p_{\theta}(c_i \mid \theta) \cdot p_{\theta}(\theta)}{p(c_i)}$$
$$= \frac{1}{\rho(\theta_{\text{max}} - \theta_{\text{min}})} \cdot \frac{1}{\sqrt{2\pi\sigma^2}} \exp\left(-\frac{(\theta - \mu)^2}{2\sigma^2}\right)$$

This implies that the posterior distribution $p_{\theta}(\theta \mid c_i)$ is a normal distribution with mean μ and variance σ^2 :

$$p_{\theta}(\theta \mid c_i) \sim \mathcal{N}(\mu, \sigma^2)$$

Therefore, the within-class variance σ_{post}^2 of the posterior distribution is equal to σ^2 . Combining the previous result with the Hessian calculation, we can conclude that:

$$H_{\theta} = \frac{1}{\sigma^2} = \frac{1}{\sigma_{\text{post}}^2}$$

Hence, maximizing the Hessian matrix (H_{θ}) will minimize the within-class variances (σ_{post}^2) as desired.

Appendix A.3. Supporting theorems

Appendix A.3.1. Distance Preservation Theorem for Projection onto a Vector

In a 2-dimensional space with a first axis and a second axis, consider a set of points located solely on the first axis, denoted by $(x_i, 0)$, where x_i represents the position of a point along the first axis. Let $\mathbf{v} = (v_1, v_2)$ be a unit vector, with v_1 and v_2 as its components. The projection operation maps each point $(x_i, 0)$ to its corresponding scalar projection y_i onto the vector \mathbf{v} . The Distance Preservation Theorem states that the projection onto \mathbf{v} preserves the ratio of distances between the points on the first axis.

Proof: The scalar projection y_i of a point $(x_i, 0)$ onto the vector \mathbf{v} is given by:

$$y_i = \frac{(x_i, 0) \cdot \mathbf{v}}{|\mathbf{v}|} = \frac{(x_i, 0) \cdot \mathbf{v}}{1} = x_i \cdot v_1 + 0 \cdot v_2 = x_i \cdot v_1$$

This implies that the projection of each point $(x_i, 0)$ from the first axis onto the vector \mathbf{v} is obtained by multiplying the coordinate x_i by the first component v_1 of \mathbf{v} .

Now, considering the distances between two points $(x_i, 0)$ and $(x_j, 0)$ on the first axis and their corresponding projections y_i and y_j onto the vector \mathbf{v} , we define the distance between $(x_i, 0)$ and $(x_j, 0)$ as:

$$d_1 = |x_i - x_i|$$

Similarly, the distance between y_i and y_j is defined as:

$$d_2 = |y_i - y_i|$$

Substituting the expressions for y_i and y_j derived earlier, we have:

$$d_2 = |x_i \cdot v_1 - x_j \cdot v_1| = |v_1| \cdot |x_i - x_j|$$

It can be observed that the ratio of the distances is constant:

$$\frac{d_2}{d_1} = \frac{|v_1| \cdot |x_i - x_j|}{|x_i - x_j|} = |v_1|$$

This shows that the ratio of distances between the points on the first axis is preserved in the projection onto \mathbf{v} .

Therefore, the Distance Preservation Theorem for Projection onto a Vector concludes that the projection operation onto the vector $\mathbf{v} = (v_1, v_2)$ in a 2-dimensional space preserves the ratio of distances between the points on the first axis.

Appendix A.3.2. Variance Preservation Theorem for Projection onto a Vector

Consider an arbitrary subset of points located on the first axis, denoted by $X = \{x_1, x_2, \dots, x_n\}$, with a mean μ_X and variance σ_X^2 . These points are projected onto the vector $\mathbf{v} = (v_1, v_2)$ using the projection operation defined earlier.

The projected subset of points on \mathbf{v} is denoted by $Y = \{y_1, y_2, \dots, y_n\}$, where each y_i represents the projection of x_i onto \mathbf{v} . The variance of Y, denoted as σ_Y^2 , is a measure of the spread of the projected points around its mean μ_Y .

The Variance Preservation Theorem states that the ratio of variances between the projected subset Y and the original subset X is equal to the square of the first component v_1 of the projection vector \mathbf{v} .

Mathematically, this can be expressed as:

$$\frac{\sigma_Y^2}{\sigma_X^2} = v_1^2$$

Proof:. The variance of Y can be computed as:

$$\sigma_Y^2 = \frac{1}{n-1} \sum_{i=1}^n (y_i - \mu_Y)^2$$

Similarly, the variance of X can be computed as:

$$\sigma_X^2 = \frac{1}{n-1} \sum_{i=1}^n (x_i - \mu_X)^2$$

According to the Distance Preservation Theorem for Projection onto a Vector, the squared distances between the points on the first axis and their projections can be related as:

$$(y_i - \mu_Y)^2 = |y_i - \mu_Y|^2 = (|v_1| \cdot |x_i - \mu_X|)^2 = v_1^2 \cdot (x_i - \mu_X)^2$$

Substituting this expression into the variance of Y, we have:

$$\sigma_Y^2 = \frac{1}{n-1} \sum_{i=1}^n v_1^2 \cdot (x_i - \mu_X)^2 = v_1^2 \cdot \frac{1}{n-1} \sum_{i=1}^n (x_i - \mu_X)^2 = v_1^2 \cdot \sigma_X^2$$

Therefore, we have shown that:

$$\sigma_Y^2 = v_1^2 \cdot \sigma_X^2$$

Hence, the ratio of variances between the projected subset Y and the original subset X is given by v_1^2 , as stated in the Variance Preservation Theorem for Projection onto a Vector.

Appendix A.3.3. Variance Ratio Preservation Theorem for Projection onto a Vector

Consider an arbitrary subset of points located on the first axis, denoted by $X = \{x_1, x_2, \dots, x_n\}$, with variances $\sigma_{X_1}^2$ and $\sigma_{X_2}^2$ for subsets X_1 and X_2 , respectively. These points are projected onto the vector $\mathbf{v} = (v_1, v_2)$ using the projection operation defined earlier.

The projected subsets of points on \mathbf{v} are denoted by $Y_1 = \{y_1, y_2, \dots, y_n\}$ and $Y_2 = \{z_1, z_2, \dots, z_n\}$, where each y_i and z_i represents the projection of x_i onto \mathbf{v} . The variances of Y_1 and Y_2 , denoted as $\sigma_{Y_1}^2$ and $\sigma_{Y_2}^2$ respectively, measure the spread of the projected points around their respective means.

The Variance Ratio Preservation Theorem states that the ratio of variances between the projected subsets Y_2 and Y_1 is equal to the ratio of variances between the original subsets X_2 and X_1 .

Mathematically, this can be expressed as:

$$\frac{\sigma_{Y_2}^2}{\sigma_{Y_1}^2} = \frac{\sigma_{X_2}^2}{\sigma_{X_1}^2}$$

Proof:. By the Variance Preservation Theorem for Projection onto a Vector, we know that the variance of the projected subset Y can be expressed as:

$$\sigma_Y^2 = v_1^2 \cdot \sigma_X^2$$

Applying this theorem to Y_1 and X_1 , we have:

$$\sigma_{Y_1}^2 = v_1^2 \cdot \sigma_{X_1}^2$$

Similarly, applying the theorem to Y_2 and X_2 , we have:

$$\sigma_{Y_2}^2 = v_1^2 \cdot \sigma_{X_2}^2$$

Now, we can take the ratio of these variances:

$$\frac{\sigma_{Y_2}^2}{\sigma_{Y_1}^2} = \frac{v_1^2 \cdot \sigma_{X_2}^2}{v_1^2 \cdot \sigma_{X_1}^2} = \frac{\sigma_{X_2}^2}{\sigma_{X_1}^2}$$

Therefore, we have shown that the ratio of variances between the projected subsets Y_2 and Y_1 is equal to the ratio of variances between the original subsets X_2 and X_1 , as required.

Appendix B. Multidimensional extension of Theorem 1 for maximizing squared between-class mean distance via eigenanalysis of the covariance matrix

To extend Theorem 1 to multidimensional data, we consider a dataset where each sample is represented by a D-dimensional column vector $\vec{\theta} = [\theta_1, \theta_2, \cdots, \theta_D]^T$. The dataset of 2n samples is divided into two subsets: $C_1 = \{\vec{x}_i \in \mathbf{R}^D \mid i=1,2,\ldots,n\}$ and $C_2 = \{\vec{y}_j \in \mathbf{R}^D \mid j=1,2,\ldots,n\}$, each containing n samples. The data in C_1 and C_2 follow the same underlying distribution, centered around their respective means, \vec{m}_1 and \vec{m}_2 , resulting in the combined data from C_1 and C_2 being centered around an overall mean of \vec{m} . The covariances for C_1 and C_2 are equal, noted as $Cov_1 = Cov_2 = Cov_w$, and the combined data has an overall covariance of Cov. The individual distributions for the vectors \vec{X} and \vec{Y} are isotropic about their respective means, meaning their covariances are proportional to the unit matrix in D dimensions, i.e., $Cov_w = \sigma_w^2 I_D$. The distance between the class means, $d = \|(\vec{m}_1 - \vec{m}_2)\|$, indicates the separation between \vec{m}_1 and \vec{m}_2 .

Define the sample means

$$\vec{m} = \frac{1}{2n} \sum_{k=1}^{2n} \vec{\theta}_k = \frac{n}{2n} \vec{m}_1 + \frac{n}{2n} \vec{m}_2 = \frac{1}{2} (\vec{m}_1 + \vec{m}_2)$$
(B.1)

where

$$\vec{m}_1 = \frac{1}{n} \sum_{i=1}^n \vec{x}_i \text{ and } \vec{m}_2 = \frac{1}{n} \sum_{j=1}^n \vec{y}_j$$
 (B.2)

The biased sample covariance matrix of the combined training set is then given by

$$Cov = \frac{1}{2n} \sum_{k=1}^{2n} (\vec{\theta}_k - \vec{m}) (\vec{\theta}_k - \vec{m})^T = \frac{1}{2n} \sum_{k=1}^{2n} \vec{\theta}_k \vec{\theta}_k^T - \vec{m}\vec{m}^T$$
 (B.3)

Expanding this yields

$$Cov = \frac{1}{2n} \left[\sum_{i=1}^{n} \vec{x}_i \vec{x}_i^T + \sum_{j=1}^{n} \vec{y}_j \vec{y}_j^T \right] - \vec{m} \vec{m}^T$$
 (B.4)

Now,

$$\sum_{i=1}^{n} \vec{x}_{i} \vec{x}_{i}^{T} = \sum_{i=1}^{n} \vec{x}_{i} \vec{x}_{i}^{T} - (n) \vec{m}_{1} \vec{m}_{1}^{T} + (n) \vec{m}_{1} \vec{m}_{1}^{T} = n \left(Cov_{1} + \vec{m}_{1} \vec{m}_{1}^{T} \right)$$
(B.5)

and similarly

$$\sum_{j=1}^{n} \vec{y}_{j} \vec{y}_{j}^{T} = n \left(Cov_{2} + \vec{m}_{2} \vec{m}_{2}^{T} \right)$$
(B.7)

where C_1 and C_2 are the (biased) sample covariances of the class 1 and class 2 subsets respectively. Substituting (B.1), (B.5), and (B.7) in (B.4), after some algebra, leads to

$$Cov = \frac{n}{2n}Cov_1 + \frac{n}{2n}Cov_2 + \frac{n^2}{(2n)^2}(\vec{m}_1 - \vec{m}_2)(\vec{m}_1 - \vec{m}_2)^T = Cov_w + \frac{1}{4}(\vec{m}_1 - \vec{m}_2)(\vec{m}_1 - \vec{m}_2)^T$$
(B.8)

It reduces to the result of Theorem 1 for D = 1. To see this, take the trace of (B.8) to show that

$$\operatorname{tr}(Cov) = \operatorname{tr}(Cov_w) + \frac{1}{4}\operatorname{tr}\left((\vec{m}_1 - \vec{m}_2)(\vec{m}_1 - \vec{m}_2)^T\right)$$
 (B.9)

But tr $(\vec{m}_1 - \vec{m}_2)(\vec{m}_1 - \vec{m}_2)^T$ = $||\vec{m}_1 - \vec{m}_2||^2$ and the trace of a diagonalizable matrix is equal to the sum of its eigenvalues, in this case the sum of the variances of the corresponding training set along the directions of the eigenvectors. So, if D = 1 then

$$\sigma^{2} = \frac{1}{2}\sigma_{1}^{2} + \frac{1}{2}\sigma_{2}^{2} + \frac{1}{4}(m_{1} - m_{2})^{2} = \sigma_{\omega}^{2} + \frac{1}{4}(m_{1} - m_{2})^{2}$$
(B.10)

which is equivalent to the result of Theorem 1. Theorem 1, however, is supposed to hold for the projection of the data onto an arbitrary 1D subspace of the full D-dimensional data space, and to imply that maximizing σ^2 by choosing the direction of this subspace appropriately will also be the direction which maximizes the difference between the projected sample means. Fortunately, since $Cov_w = \sigma^2 I_D$, we have

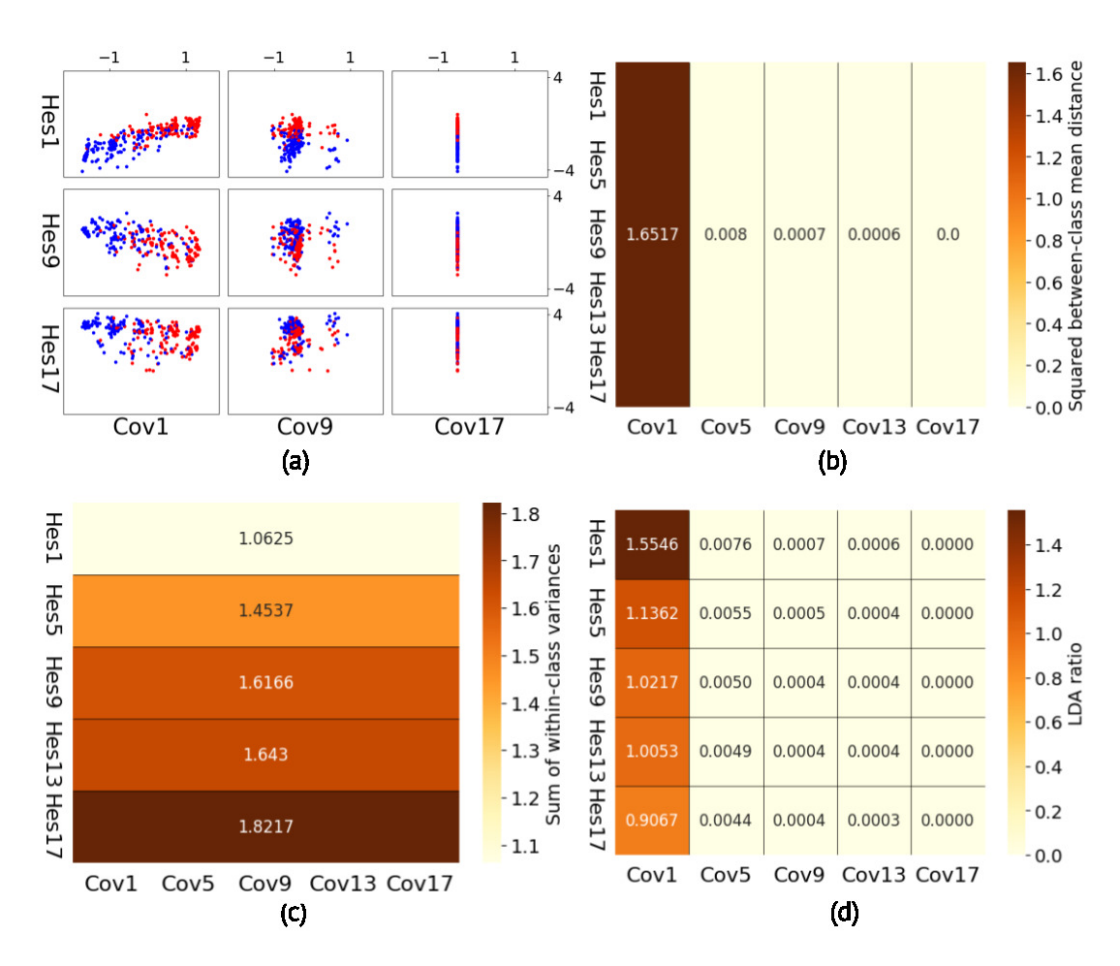
$$Cov = \sigma_w^2 I_D + \frac{1}{4} (\vec{m}_1 - \vec{m}_2) (\vec{m}_1 - \vec{m}_2)^T$$
(B.11)

Multiplying both sides with $(\vec{m}_1 - \vec{m}_2)$ yields

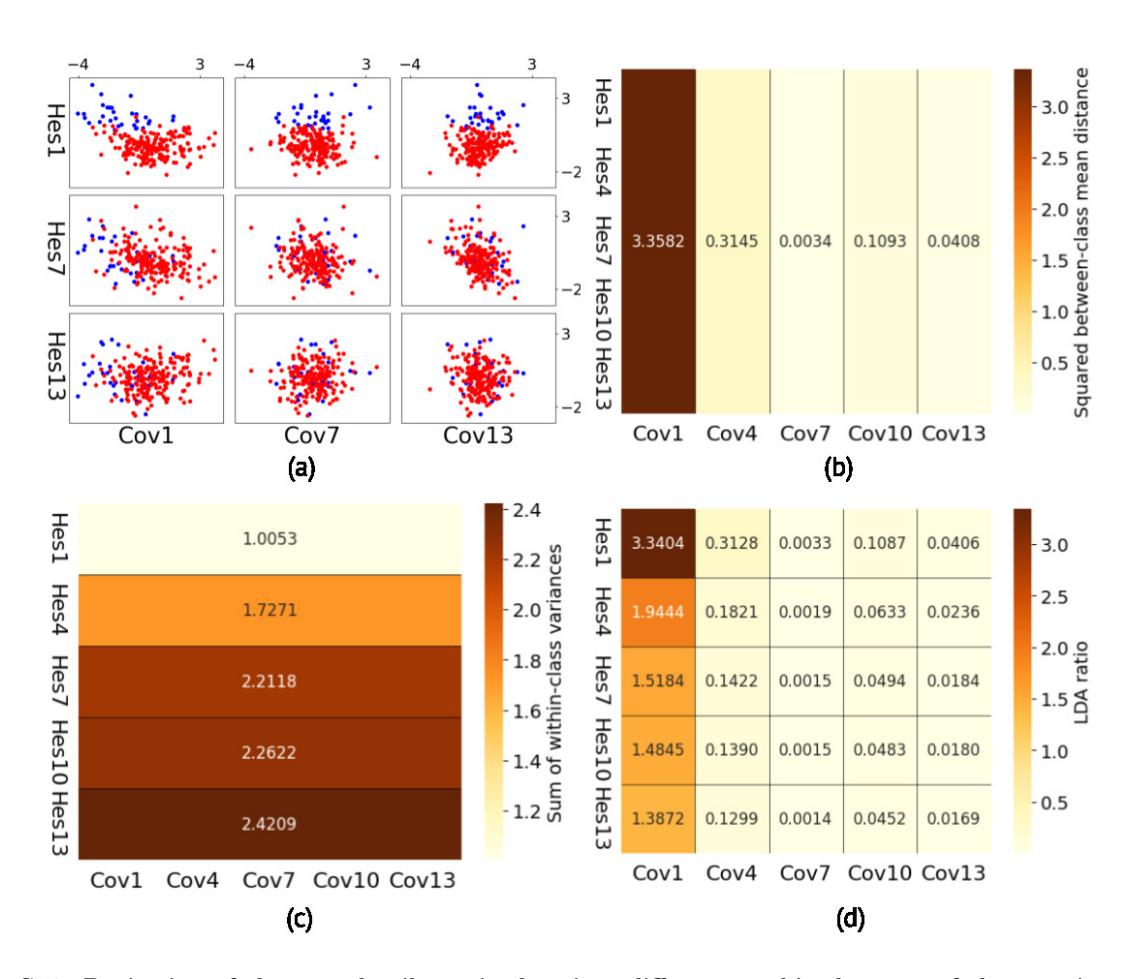
$$Cov(\vec{m}_1 - \vec{m}_2) = \left(\sigma_w^2 + \frac{1}{4}d^2\right)(\vec{m}_1 - \vec{m}_2)$$
 (B.12)

Please note that equation (B.12) forms an eigenequation where Cov is the matrix of interest, the term $\left(\sigma_w^2 + \frac{1}{4}d^2\right)$ represents the eigenvalue, and $(\vec{m}1 - \vec{m}2)$ is the eigenvector. This implies that the difference between the mean vectors $(\vec{m}1 - \vec{m}2)$ is indeed an eigenvector of the full set's covariance matrix Cov. This alignment confirms that the projection maximizing the variance in the D-dimensional space will also maximize the between-class mean distance, ensuring the validity of Theorem 1 in higher dimensions.

Appendix C. Additional dataset results



 $\label{eq:Figure C.11: Projection of the heart disease data into different combined spaces of the covariance and Hessian eigenvectors.$



 $\label{eq:Figure C.12: Projection of the neural spike train data into different combined spaces of the covariance and \\ \textbf{Hessian eigenvectors.}$

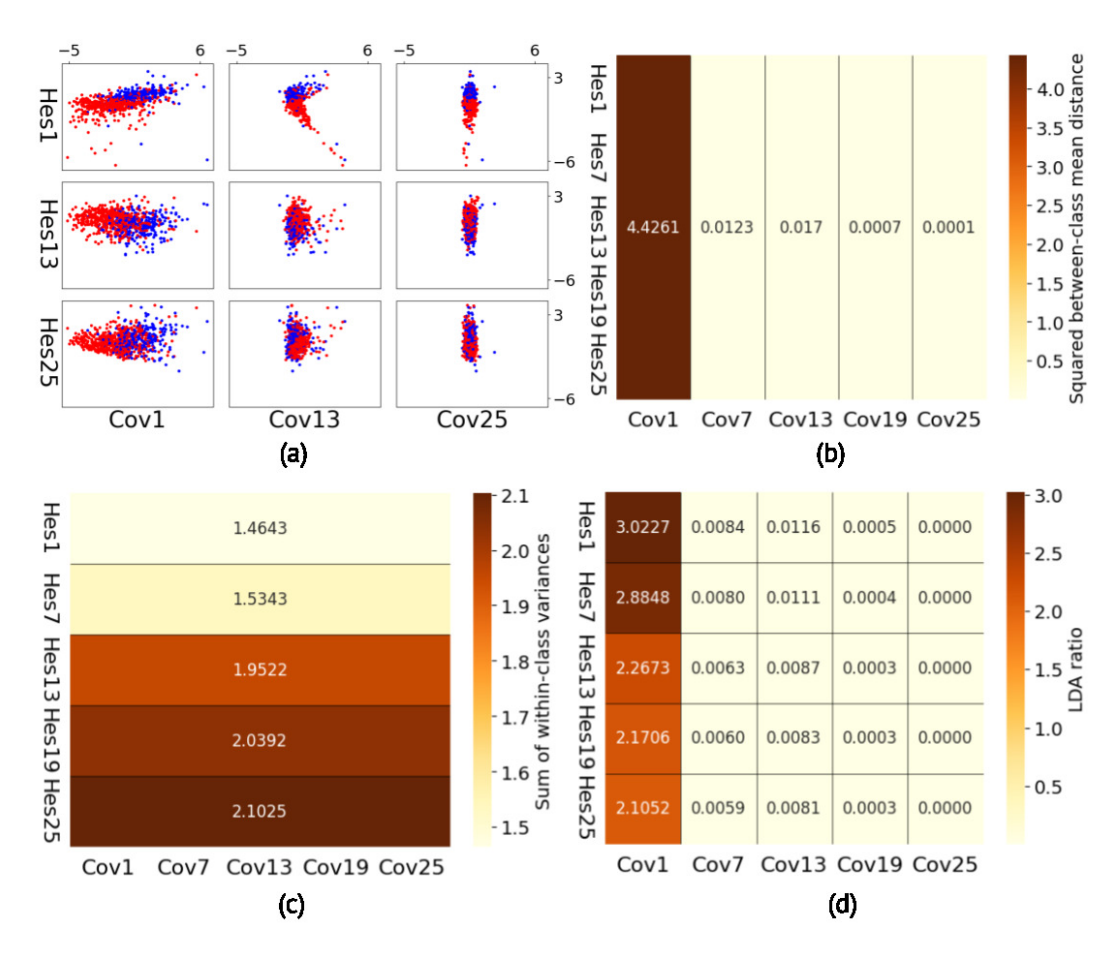


Figure C.13: Projection of the Pima Indians diabetes data into different combined spaces of the covariance and Hessian eigenvectors. (a) Nine selected projection plots, each representing data projected onto a distinct space created by combining the first three covariance and first three Hessian eigenvectors. (b) Heatmap showing the squared between-class mean distance for projections onto varying combinations of covariance and Hessian eigenvectors. (c) Heatmap showing the sum of within-class variances for projections onto different combinations of covariance and Hessian eigenvectors. (d) Heatmap displaying the LDA ratio, representing the ratio between the squared between-class mean distances presented in (b) and the corresponding within-class variances shown in (c).